LA-UR-15-27057
Approved for public release; distribution is unlimited.

Title: A Calibration to Predict the Concentrations of Impurities in Plutonium Oxide by Prompt Gamma Analysis Revision 2

Author(s): Narlesky, Joshua Edward
Kelly, Elizabeth J.

Intended for: Report

Issued: 2015-09-10

A Calibration to Predict the Concentrations of Impurities in Plutonium Oxide by Prompt Gamma Analysis Revision 2

Joshua E. Narlesky and Elizabeth J. Kelly

September 1, 2015

Introduction

Prompt gamma (PG) analysis is a nondestructive, nuclear, elemental analysis technique that uses charged particle reactions to interrogate a sample, and elements present in the sample matrix are identified through the characteristic gamma-rays emitted from the product nuclei. Plutonium oxide materials self-interrogate with the nominally 5-MeV alpha-particles that are emitted from ^{238}Pu, ^{239}Pu, ^{240}Pu, and ^{241}Am, and alpha-particle induced reactions have been observed for a set of light-elements mixed within a plutonium oxide matrix [1,2].

This technique has been applied to containers of plutonium oxide packaged in DOE Standard 3013 containers for long-term storage to identify the light elements present. A set of calibration equations have been developed between the normalized peak areas obtained from the PG analysis and the concentration of the light elements measured by analytical chemistry [3]. Ordinary least squares (OLS) models indicated that the variability in the data increases as a function of concentration. In addition, the data points at higher concentration have a larger influence on the regression. Therefore, a log-log transform was used to stabilize the variability in the data. This resulted in models in the form of a power function. The power function models provided a reasonable fit of the data, but the prediction intervals were not meaningful due to the large size, particularly at high concentration.

This paper describes a new approach using weighted least squares (WLS) regression. In this method, each data point is given its proper amount of influence over the parameter estimates. This gives two big advantages, more precise parameter estimates and better and more defensible estimates of uncertainties [4,5]. The continued destructive evaluation of 3013 containers has provided additional analytical chemistry measurements leading to larger data sets for the sensitive elements. Trends within some data sets have been recognized, such as lower variability in the data set containing materials with greater than 72 wt% actinide that also have uranium concentrations of less than 3E+05 micrograms of uranium per gram of plutonium. Models have been obtained for these subsets and may be used in limited cases to obtain estimates of impurity concentration with lower uncertainty than the WLS models for the complete data set.

Many of the alpha-particle-induced reactions produce multiple gamma-rays. The calibration equations were obtained using the gamma-ray peaks carefully chosen by considering the intensity as well as other possible interferences in the region of interest (ROI). As part of this work, we have obtained relative intensities for other gamma-rays that may be used.

Data and Methods

Extensive studies have identified that certain isotopes undergo alpha-particle-induced reactions that emit prompt gamma-rays, making those elements detectable in

plutonium oxides [1,2,6] by NDA. The elements detectable in plutonium oxides are shown in Table 1 along with the reaction and gamma-ray used for analysis. The table also provides the detection limit ($LLD_{60\ min}$) for each element in plutonium oxide based on its detection with the given gamma-ray with a 60-minute counting time [3]. The detection limits are given on the element basis but may be converted to the isotope basis by multiplying by the isotopic abundance. Table 1 also lists the gamma-ray produced by the alpha-particle-induced reaction and the most reliable gamma-ray peak that is used for identification and quantification. Many of the alpha-particle-induced reactions produce multiple gamma-rays, and those that are useful for identification and quantification are discussed later. The right-most column indicates whether the prompt-gamma data may be used to estimate the concentration of these elements in the material matrix.

TABLE 1. LIGHT ELEMENTS SENSITIVE TO PG ANALYSIS AND CORRESPONDING REACTIONS AND GAMMA-RAYS USED FOR DETECTION

Element	Reaction	Gamma-ray (MeV)	Isotopic Abundance (%)	Element $LLD_{60\ min}$ (%)	Quantitative
Lithium	$^{7}Li(\alpha,\alpha'\gamma)^{7}Li$	0.478	92.5%	0.026%	No
Beryllium	$^{9}Be(\alpha,n\gamma)^{12}C$	4.439	100.0%	0.008%	**Yes**
Boron	$^{10}B(\alpha,p\gamma)^{13}C$	3.684	19.9%	0.046%	No
Nitrogen	$^{14}N(\alpha,p\gamma)^{17}O$	0.871	99.6%	No data	No
Oxygen	$^{18}O(\alpha,n\gamma)^{21}Ne$	2.438	0.2%	13.0%	No
Fluorine	$^{19}F(\alpha,n\gamma)^{22}Na$	0.891	100.0%	0.200%	**Yes**
Sodium	$^{23}Na(\alpha,p\gamma)^{26}Mg$	1.809	100.0%	0.014%	**Yes**
Magnesium	$^{25}Mg(\alpha,n\gamma)^{29}Si$	1.779	10.0%	0.056%	**Yes**
Aluminum	$^{27}Al(\alpha,p\gamma)^{30}Si$	2.236	100.0%	0.130%	**Yes**
Silicon	$^{28}Si(\alpha,p\gamma)^{31}P$	2.234	92.2%	No data	No
Phosphorus	$^{31}P(\alpha,p\gamma)^{34}S$	2.127	100.0%	0.820%	**Yes**
Chlorine	$^{35}Cl(\alpha,p\gamma)^{38}Ar$	2.168	75.8%	0.640%	**Yes**
Potassium	$^{39}K(\alpha,p\gamma)^{42}Ca$	1.524	93.3%	2.0%	**Yes**

Prompt Gamma Data

Prompt gamma analysis is performed on plutonium-bearing materials, packaged in DOE Standard 3013 containers for long-term storage. The containers are counted using high-resolution, coaxial high-purity germanium detectors as part of the nondestructive analysis (NDA) process. The gamma-ray spectrum files are analyzed with Prompt Gamma Analysis (PGA) Software developed at Los Alamos National Laboratory [7]. The analysis software reads the raw spectrum files, performs an energy calibration, locates all peaks in the spectrum, determines the area under each peak, and computes the normalized peak areas for the peaks that correspond with alpha-particle-induced

reactions. The software then identifies the sensitive light elements present in the material based on the characteristic gamma-rays observed in the spectrum, and provides the necessary data records.

The normalized peak areas PG_i are unitless quantities and are obtained by determining the net counts P_i for a given peak and dividing by the normalization factor n and the attenuation factor A_i as shown in Eq. (1). The net counts were obtained by determining the gross counts G_i and subtracting the average background B_i. The gross counts are the sum of the counts c in the ROI containing the j channels corresponding to the peak.

$$PG_i = \frac{P_i}{n \cdot A_i} = \frac{G_i - B_i}{n \cdot A_i} = \frac{\sum_{j\,\text{channels}} c_j - B_i}{n \cdot A_i} \tag{1}$$

The normalization factor is obtained from the net counts from the ^{239}Pu gamma-ray peak at 0.414 MeV ($n_{414\ kev}$) and the ^{241}Am gamma-ray peak at 0.662 MeV ($n_{662\ kev}$), as shown in Eq. (2)

$$n = \left(\frac{n_{414\,\text{kev}}}{A_{414\,\text{kev}}} \cdot \frac{S_{Pu-239}}{s_{\text{Pu-239}}} + \frac{n_{662\,\text{kev}}}{A_{662\,\text{kev}}} \cdot \frac{S_{Am-241}}{s_{\text{Am-241}}} \right) 10^{-6} \ \ [\text{counts}], \tag{2}$$

where S_{Pu-239} and S_{Am-241} are the specific alpha activities of ^{239}Pu and ^{241}Am and s_{Pu-239} and s_{Am-241} are the specific gamma activities of ^{239}Pu at 0.414 MeV and ^{241}Am at 0.662 MeV, respectively. The attenuation factor A_i is applied to correct for the differences in thickness for the various container configurations that may be counted. For example, the material may be counted in its packaged state in the 3013 container, which is a nested configuration consisting of the outer 3013 container, the inner container, and the convenience container, or it may be counted in just the convenience container. For a given container configuration, the attenuation factor is calculated from Eq. (3)

$$A_i = \exp\left[-\left(\mu / \rho \right)_i \cdot \rho \cdot t \right], \tag{3}$$

where the quantity (μ/ρ) is the mass attenuation coefficient for the steel for the energy of gamma-ray peak i, ρ is the density of the steel, and t is the total wall thickness of the steel containers.

Various absorbers had been used to shield the counting system from the low-energy gamma-rays from ^{241}Am to reduce the dead time. Historically, the use of absorbers has not been recorded; however, and equivalent thickness of lead may be determined empirically using the ratio χ of the ^{239}Pu gamma-ray peak at 0.414 MeV to the ^{239}Pu gamma-ray peak at 0.646 MeV. It has been demonstrated that values of χ less than or

equal to 39 indicate that the attenuation is significant, and a correction must be applied.[14] This is done by determining the absorber thickness *t* from the χ using Eq. (4).

$$t = 1.26 - 0.31 \cdot \ln(\chi) \ \ (\chi < 39) \ \text{[in]}$$
$$t = 0 \ \ (\chi \geq 39) \qquad (4)$$

The attenuation caused by the absorbers (if present) can then be calculated using Eq. (3) substituting the appropriate density and the mass attenuation coefficients for each gamma-ray peak.

Analytical Chemistry Data

The regression analysis used to obtain calibration equations was performed on data obtained from standards, which have both analytical chemistry and PG analysis data [3]. The standards are part of the same population of materials packaged in 3013 containers and belong to one of the following three groups:

1. Samples in the Materials Identification and Surveillance (MIS) program. These samples were obtained from the various DOE sites before thermal stabilization for packaging according to the 3013 standard. This group of samples as a whole is considered representative of all the materials packaged in 3013 containers,
2. Samples of thermally stabilized material destructively analyzed at the DOE packaging sites, and
3. Samples obtained during the destructive analysis of 3013 containers after storage for a prescribed period of time.
4. Oxide materials produced in the magnesium hydroxide precipitation process from PUREX product quality nitrate solution. Analytical chemistry for the feed items indicates that the total impurities are generally less than one percent. Analytical chemistry is not available on the oxide materials, but the magnesium concentration can be calculated based on the assumption that the major components are plutonium oxide and magnesium oxide. The plutonium oxide concentration is available from NDA.

The analytical chemistry and PG data from the standards were evaluated for inclusion in the regression model based on several factors, which include the distribution of the light elements in the material matrix, the measurement conditions for analytical chemistry and PG analysis, and the analytical chemistry technique used. The analytical chemistry methods and data selection process was described in detail in the previous report [3]. The updated information for the standards is given in Table 2.

TABLE 2. STANDARDS USED IN THE REGRESSION ANALYSIS

Standard Type	No. of Standards in Data Set	No. of Analytical Chemistry Measurements	Material Stabilization Temperature†	Analytical Method	Sample Preparation Method	Al	B	Be	Cl	F	Li	Mg	P	K	Na	Si
Representative Items in MIS Program	49	14/49	As received by LANL*	ICP-AES / ICP-MS	HNO_3/HF Dissolution	Y	Y	Y			Y	N	Y	N	N	Y
				Ion Chromatography	Pyrohydrolysis				N	N						
		1/49	600ºC*	ICP-AES / ICP-MS	HNO_3/HF Dissolution	Y	Y	Y			Y	N	Y	N	N	Y
				Ion Chromatography	Pyrohydrolysis				N	N						
		1/49	800ºC*	ICP-AES / ICP-MS	HNO_3/HF Dissolution	Y	Y	Y			Y	Y	Y	Y	Y	Y
				Ion Chromatography	Pyrohydrolysis				Y	Y						
		35/49	950ºC*	ICP-AES / ICP-MS	HNO_3/HF Dissolution	Y	Y	Y			Y	Y	Y	Y	Y	Y
				Ion Chromatography	Pyrohydrolysis				Y	Y						
Hanford 3013 Container	16	16/16	750-950ºC*	Ion Chromatography	Water Leach				N	N						
				Ion Selective Electrode	Na_2O_2-NaOH Fusion					N						
				ICP-AES / ICP-MS	Acid Leach	N	N	N			N	Y	N	Y	Y	N
				ICP-AES / ICP-MS	Na_2O_2-NaOH Fusion	Y	Y	Y			Y	Y	Y	N	N	Y
Hanford Input Item	12	1/12	Not Stabilized*	Volhard Titration	Water Leach				Y							
		4/12	Not Stabilized*	Ion Selective Electrode	Water Leach				Y							
		7/12	Not Stabilized*	ICP-AES / ICP-MS	$NaHSO_3$ Fusion	Y	Y	Y			Y	Y		Y		Y
Hanford MGO Material	63	63/63	950ºC	Mg conc. calculated from total actinide conc. by NDA	n/a							Y				
Rocky Flats Input Item	11	11/11	Not Stabilized*	ICP-AES	not reported							Y		Y	Y	
		11/11	Not Stabilized*	not reported	not reported				Y							
Savannah River Site 3013 Container	24	24/24	750-950ºC*	ICP-AES / ICP-MS	HNO_3/HF Dissolution	Y	Y	Y			Y	Y	Y	Y	Y	Y
		16/16		Ion Chromatography	Pyrohydrolysis				Y	Y						
3013 Container Destructive Analysis	83	83/83	750-950ºC*	Ion Chromatography	Acid Leach				Y	N						
		83/83		ICP-AES	Acid Leach	N		N				N		Y	Y	
		23/83		ICP-AES	HNO_3 Dissolution	Y		Y				Y		Y	Y	
		83/83	750-950ºC*	ICP-AES	HNO_3/HBO_3 Dissolution	Y		Y				Y		Y	Y	
		8/83	750-950ºC*	Ion Chromatography	Na_2O_2-H_2SO_4 Fusion				Y	Y						
		8/83	750-950ºC*	ICP-AES	Na_2O_2-H_2SO_4 Fusion	Y		Y				Y				Y
		2/83	750-950ºC*	Ion Chromatography	HNO_3/KF Dissolution				Y	Y						
		2/83	750-950ºC*	ICP-AES	HNO_3/KF Dissolution	Y						Y			Y	

* Based on the processing history and the physical condition of the material, it is evident that the chloride salt components were at one time heated above their respective melting temperatures.

† The material stabilization temperature indicates the stabilization temperature of the material before analytical chemistry was performed. PG analysis was also performed on the bulk material, which had the same stabilization conditions as the aliquots used for analytical chemistry. The only exceptions are the MIS standards for which PG analysis was performed after the bulk mateial was calcined at 950ºC.

Weighted Least Squares Models of PG and Analytical Chemistry

Previous work has shown that the variability of PG data increases with concentration. A method such as OLS that treats all of the data equally would give less precisely measured points more influence than they should have and would give highly precise points too little influence. In addition, larger values tend to have greater influence than smaller values. Therefore, it is not reasonable to assume that every observation should be treated equally. Weighted least squares can be used to optimize parameter estimation by giving each data point its proper amount of influence over the parameter estimates, and there is scientific justification for decreased precision at higher concentration. The WLS method can apply weight factors to the observations so that the observations with larger values of concentration have less influence. This gives two big advantages: more precise parameter estimates and better and more defensible estimates of uncertainties [4,5].

The prompt gamma normalized peak area *PG* and the analytical chemistry data *C* are being fit to a model of the form shown in Eq. (5)

$$PG_k = \beta C_k + \varepsilon \tag{5}$$

where ε is the random error term. This model will result in a straight line through the origin with a slope β. The parameter is essentially the sensitivity: unit of signal per ppm concentration. It is assumed that the prompt gamma signal is zero at a concentration of zero. In OLS, the residual sum of squares *RSS* is minimized to find the parameter β in Eq. (6)

$$RSS = \sum_{k=1}^{m} \left(PG_k - C_k * \beta \right)^2 , \tag{6}$$

where *m* is the sample size. In this case the variance of ε is assumed to be constant for all C_k. In weighted least squares regression, *RSS* is weighted by weight factor w_i to give the weighted residual sum of squares *WSS* in Eq. (7).

$$WSS = \sum_{k=1}^{m} w_k \left(PG_k - C_k * \beta \right)^2 \tag{7}$$

This expression is equivalent to *RSS* in OLS when all w_k are equal to 1. In the WLS model, we chose weight factors equal to $1/C_k$ because the data indicate variances proportional to C_k. When the weight factors are applied, the assumption of constant variance holds true.

The standard error for the weighted regression se_w was determined from Eq. (8)

$$se_w = \left[\sum_{k=1}^{m} \left(PG_k - \overline{PG_w} \right)^2 - \frac{\left(\sum_{k=1}^{m} \left(C_k - \overline{C_w} \right) \left(PG_k - \overline{PG_w} \right) \right)^2}{\sum_{k=1}^{m} \left(C_k - \overline{C_w} \right)^2} \right] \Big/ df \tag{8}$$

where the degrees of freedom $df = m - 1$ because the intercept term is not used. The terms $\overline{PG_w}$ and $\overline{C_w}$ are the weighted averages of the prompt gamma data and analytical chemistry data, respectively.

For a new observation PG_0, the chemistry value is then obtained using the inverse calibration shown in Eq. (9).

$$C_0 = \frac{1}{\beta} \cdot PG_0 \tag{9}$$

The standard error associated with C_0 is given by Eq. (10)

$$se_{C_0} = \frac{se}{\beta} \sqrt{\frac{1}{w_0} + \frac{1}{\sum w_i} + \frac{\left(PG_0 - \overline{PG_w} \right)^2 \sum w_i}{\beta^2 \left(\sum w_i \sum w_i C_i^2 - \left(\sum w_i C_i \right)^2 \right)}} \tag{10}$$

where $w_0 = 1/C_0$.

The two-sided confidence intervals for C_0 are then given by Eq. (11)

$$CI_0^{\pm} = C_0 \pm t\left(m-1,\ \alpha/2\right) \cdot se_{C_0} \tag{11}$$

where $t\left(m-1,\ \alpha/2\right)$ is the *t*-distribution with degrees of freedom $df = m - 1$ and probability $\alpha/2$ (the desired confidence level). Although denoted as confidence intervals, these may be used as inverse prediction limits. These limits correspond to selecting two limits $C_0^{\pm}$, which are derived from the prediction uncertainties on PG_0. The term C_0^- is the analytical chemistry value where the lower prediction limit for PG_0 intersects the upper prediction uncertainty equation, and C_0^+ is the value where the upper prediction limit intersects the lower prediction uncertainty equation.

Results and Discussion

The WLS method was used to fit the prompt gamma data *PG* and the analytical chemistry data *C* to a linear model of the form shown in Eq. (5) for beryllium, fluorine, sodium, magnesium, aluminum, phosphorus, chlorine, and potassium. The fits were then used to obtain inverse

calibration equations as shown in Eq. (9) to estimate the concentration of these elements from *PG* using the inverse sensitivity $1/\beta$.

The data set used for each fit was refined by identifying statistical outliers, and excluding certain outliers, based on physical explanation. Statistical outliers were identified using the Normal Q-Q and the Cook's distance plots. The Cook's distance plot was used to identify data points with more than average influence on the model. The Cook's distance plot generally identified outliers with large values of *C* and/or *PG.* The statistical outliers were then evaluated to determine if there was an underlying physical explanation for why these observations differed from the rest of the data. Physical explanations include poor mixing and low signal-to-noise ratios. Those statistical outliers that were also deemed physical outliers were not used to determine the calibration equation. A cautionary note is that when using the calibration equations, one needs to make sure that the prompt gamma measurements themselves are not outliers and are not affected by poor mixing or low signal-to-noise ratios.

As stated earlier, multiple gamma-rays may be generated from a given reaction, resulting in multiple gamma-ray peaks in different regions of the spectrum for a given element. These gamma-ray peaks may be integrated, and the normalized count data may be used in lieu of or in addition to the normalized count data from the standard gamma-ray peak to obtain concentration estimates. When using gamma-ray peaks other than the standard peak, the normalized count data must be corrected by the relative intensity with respect to the standard peak as shown in Eq. (12).

$$PG = \frac{PG_j}{I_{j:s}} \tag{12}$$

where *PG* is the adjusted normalized count data, $I_{j:s}$ is the relative intensity of gamma-ray peak *j* with respect to the standard peak *s*, and PG_j is the normalized count data for the nonstandard gamma-ray peak. Relative intensities obtained from gamma-ray spectra of pure target materials bombarded with 5 MeV alpha particles are available in the literature [6]. We compared those relative intensities with those observed for our materials to evaluate the effect of actinide interferences and interferences of other reaction gamma-rays. The gamma-ray peaks whose relative intensities do not match the reported values in the literature due to interferences have been excluded.

Chlorine

Natural occurring isotopes of chlorine include ^{35}Cl (76%) and ^{37}Cl (24%). Alpha-particle-induced reactions with the isotopes of chlorine produce multiple gamma-rays, but only the 2.168 MeV peak from the ^{35}Cl(α,p) reaction was observed in the gamma-ray spectra for the standards. The 2.168 MeV peak is used as the standard peak for use in the calibration. The ROI for this gamma-ray peak is free of interference.

A fit of the normalized count data and the chemistry data for chlorine was obtained using 94 data points. Based on the Cook's Distance diagnostic, two data points were identified as

potential outliers, both having high values of *C* where poor mixing is possible. However, the outliers were not removed from the fit because their overall effect was minimal.

A plot of the calibration equation with uncertainties for the gamma-ray peak at 2.168 MeV is provided in Figure A.1 of Appendix A. The regression line is given by Eq. (13).

$$C_{Cl} = 1.099 \times 10^{7} \cdot PG_{2.168\,MeV} \tag{13}$$

Uncertainties in the calibration can be reduced by refining the data set. This was done by selecting materials having the best possible mixing. For chlorides, this occurs for materials with a high plutonium and americium alpha source term with respect to the chloride and low uranium. For the packaged materials, the best mixing is typically observed in materials with or equal to or greater than 72 wt% actinide with less than 3E+05 micrograms of uranium per gram of plutonium. This group of materials has higher concentrations of 5-MeV alpha-particle emitters and is referred to as the "RICH" data set. A plot of the calibration equation with uncertainties for the gamma-ray peak at 2.168 MeV for the "RICH" data set is provided in Figure A.2 of Appendix A with the confidence intervals for the fit. The regression line for this fit is given by Eq. (14).

$$C_{Cl}(RICH) = 9.065 \times 10^{6} \cdot PG_{2.168\,MeV} \tag{14}$$

This calibration equation is valid or materials meeting the following conditions: (1) have greater than or equal to 72 wt% actinides and (2) have less than 3E+05 micrograms of uranium per gram of plutonium. The slope for this line is about 18% smaller than the slope for the calibration equation for the complete data set, which indicates that the signal for these materials is stronger than average.

Sodium

Naturally occurring isotopes of sodium include only ^{23}Na. Alpha-particle-induced reactions with ^{23}Na produce multiple gamma-rays, and the 1.808 MeV peak from the ^{23}Na(α,p) reaction is the most intense gamma-ray peak for sodium and is used as the standard peak for use in the calibration. Possible interferences in the ROI include the ^{234}Pa gamma-ray peak from the ^{238}U decay series.

A fit of the normalized count data and the chemistry data for sodium was obtained using 145 data points. Based on the Cook's Distance diagnostic, two data points were identified as potential outliers. In addition, three data points were identified as potential outliers based on the Q-Q plot. Two of the potential outliers have very low values of *PG*, with low signal-to-noise ratios, and three of the potential outliers have high values of *C* where poor mixing is possible. All five potential outliers were removed from the fit.

A plot of the calibration equation with uncertainties for the gamma-ray peak at 1.808 MeV is provided in Figure A.3 of Appendix A. The regression line is given by

$$C_{Na} = 2.514 \times 10^{5} \cdot PG_{1.808\,MeV} \quad (15)$$

Likewise to the fit of chlorine, uncertainties in the calibration can be reduced by limiting the data to "RICH materials" only. A plot of the calibration equation for gamma-ray peak at 1.808 MeV for RICH materials with uncertainties is provided in Figure A.4 of Appendix A. The regression line is given by

$$C_{Na}(MOX) = 2.189 \times 10^{5} \cdot PG_{1.808\,MeV} \quad (16)$$

This calibration equation is valid or materials meeting the following conditions: (1) have greater than or equal to 72 wt% actinides and (2) have less than 3E+05 micrograms of uranium per gram of plutonium. The change in slope indicates a 13% increase in signal for these materials.

The gamma-ray spectrum for sodium also has intense gamma-ray peaks at 1.003 and 1.130 MeV that provide alternatives for the standard peak at 1.808 MeV. No interferences exist at either of these energies. The 1.003 MeV peak can be observed in gamma-ray spectra measured over the range of 0 to 1.1 MeV, which are used to determine the plutonium isotopic composition. The relative intensities of these gamma-ray peaks with respect to the standard peak at 1.808 MeV, based on our measurements and data from the literature are given in Table 3. Prompt gamma measurements based on these gamma-ray peaks would be adjusted using Eq. 12 and the appropriate relative intensity from Table 4 to obtain $PG_{1.808\,MeV}$. The sodium concentration C_{Na} is then calculated using either Eq. 15 or 16.

TABLE 3. RELATIVE INTENSITY OF GAMMA-RAY PEAKS FOR SODIUM

Gamma-ray (MeV)	Relative Intensity (measured)	Relative Intensity (literature) [6]
1.003	0.07	0.08
1.130	0.49	0.51

Magnesium

Naturally occurring isotopes of magnesium include ^{24}Mg (79%), ^{25}Mg (10%), and ^{26}Mg (11%). Alpha-particle induced reactions with these isotopes produce numerous gamma-rays, but many of the peaks in the gamma-ray spectrum coincide with peaks of other elements, such as aluminum, fluorine, sodium and silicon. The standard peak for magnesium is located at 1.779 and it produced by the ^{25}Mg(α,n) reaction. The gamma-ray peak at 1.779 MeV is the most intense peak for ^{25}Mg and the second-most intense peak for this element overall. The ROI for this gamma-ray peak includes interferences from ^{23}Na and ^{28}Si. A correction for ^{23}Na may be applied to the raw data as follows:

$$PG_{1.779\,MeV} = PG_{1.779\,MeV\_RAW} - 0.028 \cdot PG_{1.808\,MeV} \cdot \quad (17)$$

A fit of the normalized count data and the chemistry data for magnesium was obtained using 182 data points. Based on the Cook's Distance and Q-Q plot diagnostics, six data points were identified as potential outliers and removed from the fit. Reasons for lack of fit include poor mixing, low signal-to-noise ratio and uranium above the threshold of 3E+05 micrograms per gram of plutonium. The presence of uranium dilutes the alpha source in the material matrix and results in a lower signal. A portion of the data set with high concentrations of magnesium (mostly greater than 10%) includes materials produced by magnesium hydroxide precipitation of PUREX nitrate. The feed to this process was fairly pure and the product contains mostly plutonium and magnesium oxide. The scatter in this data set is largely due to inherent homogeneity of product oxide.

A plot of the calibration equation with uncertainties for the corrected data from the 1.779 MeV peak is provided in Figure A.5 of Appendix A. The regression line is given by Eq. (18).

$$C_{Mg} = 2.773 \times 10^{6} \cdot PG_{1.779\,MeV} \tag{18}$$

The fit of the magnesium data has a large uncertainty, which is due to the different chemical forms of the impurity compounds present in the material. When materials contain a chloride-salt matrix, the signal produced by the alpha-particle-induced reactions increases for all of the impurities in the material regardless of their chemical form due to the stabilization that was performed prior to packaging. The degree of contact between the impurities and the alpha source increases as the chloride salt impurities melt and create a fused mixture containing the chloride salt, the plutonium oxide grains, and any other impurities, which become trapped in the salt. In contrast, the oxide matrix has a lower degree of contact between the impurities and the alpha source even when well-mixed, and the degree of contact does not change when the material is stabilized. Because magnesium may be present in different forms, such as magnesium chloride or magnesium oxide, the strength of the signal produced by different materials with similar magnesium concentrations can vary. This effect is illustrated in Figure 1, which shows the $PG_{1.779\,MeV}$ as a function of magnesium concentration with each data point shaded according to the chlorine concentration. The yellow points are low chlorine and the dark green points are high chlorine. At high concentrations of magnesium, the points centered about the fit line are higher in chlorine, whereas the points with lower chlorine concentrations are shifted farther to the right, which indicates a lower signal due to less contact with the alpha source. This effect is not observed in elements, such as sodium, chlorine, and potassium that are present almost exclusively in the form of a chloride salt.

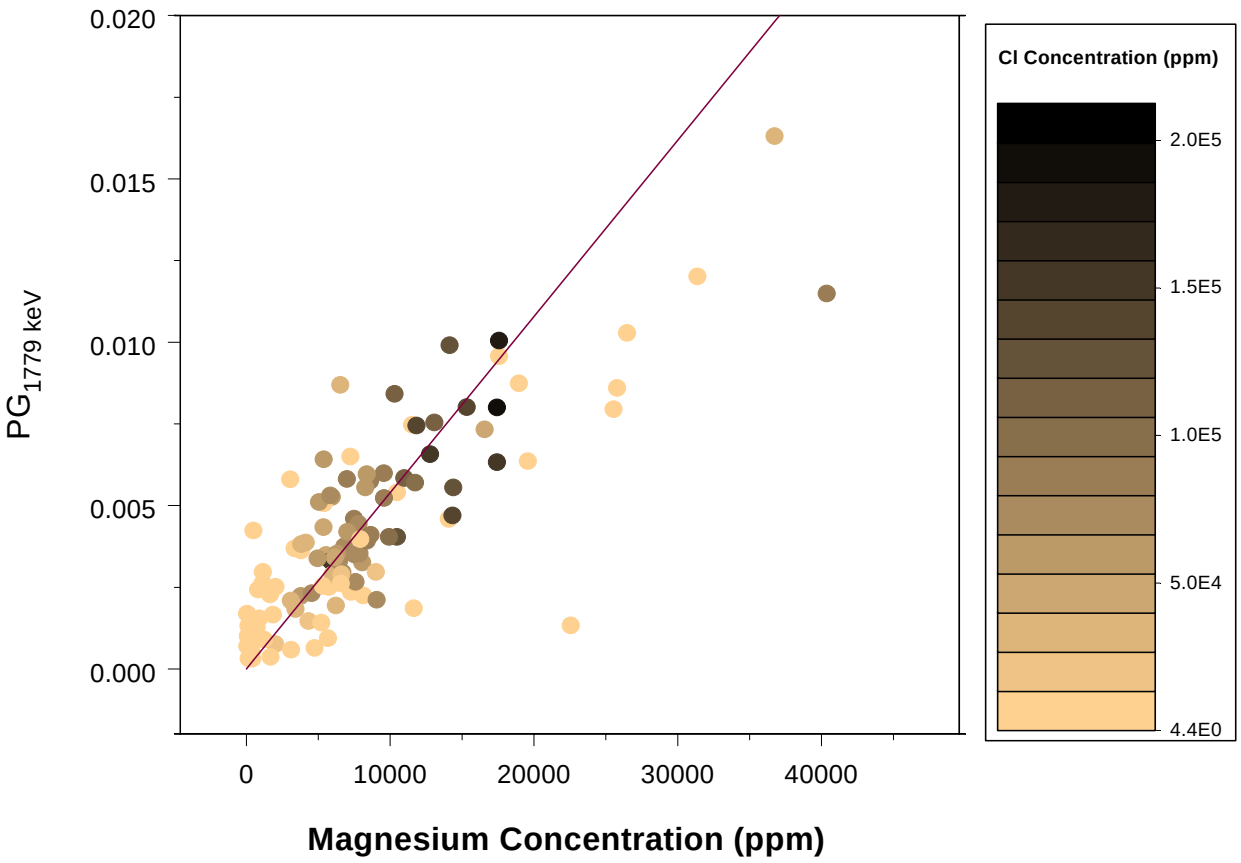

FIGURE 1. HEAT PLOT SHOWING THE CONCENTRATION (BY COLOR) OF EACH DATA POINT IN THE MAGNESIUM DATA SET (UP TO 40,000 PPM MAGNESIUM).

Uncertainties in the calibration can be reduced by separating the materials into two data sets: those having chloride salt impurities and those without chloride salt impurities. The regression lines are given by

$$C_{Mg}\,(\text{with Cl}) = 1.854 \times 10^{6} \cdot PG_{1.779\,MeV} \tag{19}$$

$$C_{Mg}\,(\text{without Cl}) = 2.821 \times 10^{6} \cdot PG_{1.779\,MeV} \tag{20}$$

A plot of the calibration equations with uncertainties for the fit of the 1.779 MeV gamma-ray peak is provided in Figure A.6 and Figure A.7 of Appendix A for materials with and without chlorine.

The slope of the regression line for materials with chloride salt impurities was reduced by about one-third from that of the complete data set, whereas the slopes for the complete data set and the set of materials without chloride salt impurities are about the same. Therefore, Eq. 19 may be used only for materials in which chlorine was detected by prompt gamma analysis due to the larger sensitivity for magnesium for that subset of materials.

The gamma-ray spectrum for magnesium also has intense gamma-ray peaks at 0.844 MeV, 1.015 MeV, 1.273 MeV, and 2.028 MeV. The gamma-ray peak at 0.844 MeV is produced in the

^{24}Mg(α,p) reaction. This gamma-ray peak has possible interference from ^{27}Al, ^{56}Fe, ^{234}Pa, and ^{239}Pu. These interferences may be significant because the relative intensity does not have good agreement with the published value as shown in Table 4. The gamma-ray peak at 1.015 MeV, produced in the ^{24}Mg(α,p) reaction may be used if analyzing plutonium isotopic spectra for the presence of magnesium. However, the interference from ^{27}Al (alpha and neutron reactions) may be significant, particularly in a high neutron field. Therefore, this gamma-ray peak should not be used if aluminum or beryllium are present. The gamma-ray peak at 1.273 MeV produced ^{26}Mg(α,n) reaction cannot be used due to the interference of ^{19}F. The gamma-ray peak at 2.028 MeV produced in the ^{26}Mg(α,n) reaction is completely free of interference from other elements and may be used as an alternative to the standard peak at 1.779 MeV. The measured relative intensity for this gamma-ray peak has the best agreement with the published value. However, using this gamma-ray peak reduces the sensitivity by a factor of five with respect to the standard peak.

TABLE 4. RELATIVE INTENSITY OF GAMMA-RAY PEAKS FOR MAGNESIUM

Gamma-ray (MeV)	Relative Intensity (measured)	Relative Intensity (literature) [6]
0.844	1.15	1.59
1.015	0.70	0.94
2.028	0.21	0.18

Beryllium

Naturally occurring isotopes of beryllium include only ^{9}Be. Alpha-particle-induced reactions with ^{9}Be produce a single gamma-ray at 4.439 MeV peak from the ^{9}Be(α,n) reaction, which is accompanied by a single and double escape peak at 3.928 MeV and 3.417 MeV, respectively. None of these gamma-ray peaks have interferences.

A fit of the normalized count data and the chemistry data for beryllium was obtained for 34 data points. Based on the Cook's Distance diagnostic, two data points were identified as potential outliers. One potential outlier has a very low value of *C.* The outlier has a relatively high value of *C* but a very low value for *PG.* The discrepancies are believed to be due to low signal-to-noise ratio and inhomogeneity of the material. The outliers had a considerable effect on the fit and were consequently removed.

A plot of the calibration equation with uncertainties for the gamma-ray peak at 4.439 MeV is provided in Figure A.8 of Appendix A. The regression line is given by

$$C_{Be} = 6.550 \times 10^{4} \cdot PG_{4.439\,MeV} \tag{21}$$

The gamma-ray spectrum for beryllium also has a single and double escape peak at 3.928 MeV and 3.417 MeV, respectively. Both gamma-ray peaks are free of interferences and may also be

used for analysis of beryllium. The relative intensities for the single and double escape peaks were obtained empirically from 3013 container data and are given in Table 5.

TABLE 5. RELATIVE INTENSITY OF GAMMA-RAY PEAKS FOR BERYLLIUM

Gamma-ray (MeV)	Relative Intensity (measured)	Relative Intensity (literature) [6]
3.417	1.00	Not available
3.928	0.86	Not available

Fluorine

Naturally occurring isotopes of fluorine include only ^{19}F. Alpha-particle-induced reactions with ^{19}F produce numerous gamma-rays, but fluorine is identified and quantified through the 0.891 MeV peak from the ^{19}F(α,n) reaction. This gamma-ray peak does not have interferences, though the signal is fairly weak with respect to other gamma-ray peaks for fluorine. Many of the higher intensity gamma-ray peaks such as the peaks at 0.197 MeV or 0.583 MeV cannot be used because they are in the heavily filtered, low-energy region of the spectrum and are difficult to distinguish from actinide gamma-ray peaks in that region.

A fit of the normalized count data and the chemistry data for fluorine was obtained for 38 data points. Based on the Cook's Distance and Q-Q plot diagnostics, two data points were identified as potential outliers, but neither data point was removed from the fit because their overall effect was minimal.

A plot of the calibration equation with uncertainties for the gamma-ray peak at 0.891 MeV is provided in Figure A.9 of Appendix A. The regression line is given by

$$C_F = 9.225 \times 10^5 \cdot PG_{0.891\,MeV} \tag{22}$$

As with many of the other elements, fluorine has multiple gamma-ray peaks in the region of the spectrum above 1 MeV. The gamma-ray peak at 1.275 MeV is produced by the ^{19}F(α,p) reaction and is more intense than the 0.891 MeV peak. However, this gamma-ray peak has interference with ^{26}Mg, which is present in much of the packaged materials, and the measured relative intensity is not in agreement with the published value, which indicates a significant interference. The gamma-ray peak at 2.081 MeV produced by the ^{19}F(α,p) reaction does not have interferences, and the measured and published relative intensities, 0.25 and 0.27 respectively, show good agreement. However, this detection limit for the 2.081 MeV peak is higher by a factor of four with respect to the 0.891 MeV peak.

Aluminum

Naturally occurring isotopes of aluminum include only ^{27}Al. Alpha-particle-induced reactions with ^{27}Al produce multiple gamma-rays, and the gamma-ray peak at 2.236 MeV from the ^{27}Al (α,p) reaction is the most intense and is used as the standard peak for analysis. Possible

interferences include the gamma-ray peak at 2.234 MeV from the ^{28}Si(α,pγ) reaction; however, because of the low sensitivity of silicon and its low concentration in the materials analyzed here, the standard peak at 2.236 MeV may be used quantitatively.

A fit of the normalized count data and the chemistry data for aluminum was obtained for 44 data points. Based on the Cook's Distance and Q-Q plot diagnostics, one data point was identified as a potential outlier and removed from the data set based on a review of the data.

A plot of the calibration equation with uncertainties for the gamma-ray peak at 2.236 MeV is provided in Figure A.10 of Appendix A. The regression line is given by

$$C_{Al} = 1.207 \times 10^{6} \cdot PG_{2.236\,MeV} \tag{23}$$

Alpha-particle-induced reactions with aluminum produce multiple gamma-ray peaks, but most of the gamma-ray peaks for aluminum are fairly weak and have interferences with other elements, such as silicon and magnesium. Interferences with silicon occur at 2.236, 1.725, 1.266, and 1.214 MeV. The interferences with magnesium occur at 0.844 and 1.015 MeV. These gamma-ray peaks have a relatively high branching ratio for magnesium and, therefore, cannot be used. Two gamma-ray peaks, 1.552 MeV and 3.498 MeV were identified as not having interferences. The gamma-ray peak at 1.552 MeV has a relative intensity of 0.021 with respect to the standard peak at 2.236 MeV and was not observed in the materials studied. The gamma-ray peak at 3.498 MeV may be used in materials with a high silicon concentration to remove the interference at the standard peak. The measured and published relative intensities for the 3.498 MeV peak, 0.17 and 0.11 respectively, show good agreement.

Phosphorus

Naturally occurring isotopes of phosphorus include only ^{31}P. Alpha-particle-induced reactions with ^{31}P produce multiple gamma-rays, and the gamma-ray peak at 2.127 MeV peak from the ^{31}P (α,p) reaction is the most intense and is used as the standard peak for analysis. Possible interferences in the 2.127 MeV region include 2.132 MeV peak from the ^{23}Na (α,p) reaction, but these two gamma-ray peaks are usually well-separated except in cases where the sodium concentration is exceptionally high.

A fit of the normalized count data and the chemistry data for aluminum was obtained for 12 data points. Based on the Cook's Distance and Q-Q plot diagnostics, two data points were identified as potential outliers, but neither of the outliers were removed from the fit due to the small size of the data set.

A plot of the calibration equation with uncertainties for the gamma-ray peak at 2.127 MeV is provided in Figure A.11 of Appendix A. The regression line is given by

$$C_{P} = 2.603 \times 10^{6} \cdot PG_{2.127\,MeV} \tag{24}$$

Additional gamma-ray-peaks for phosphorus are reported in the literature, but their relative intensity and, therefore, their sensitivity are an order of magnitude lower. None of these gamma-ray peaks were observed in the gamma-spectra for the standards due to the low concentration of phosphorus in these materials.

Potassium

Naturally occurring isotopes of potassium include ^{39}K, ^{40}K, and ^{41}K. Alpha-particle-induced reactions on the potassium isotopes produce multiple gamma-rays, and the gamma-ray peak at 1.524 MeV from the ^{39}K(α,pγ) reaction is the most intense and is used as the standard peak for analysis. The overall signal for potassium is typically very weak because it is one of the heaviest elements that undergoes (α,pγ) reaction, and the reaction cross-section is much lower for potassium than for lighter elements. Interferences in the 1.524 MeV ROI include the 1.528 MeV gamma-ray peak from fluorine. In some cases, subtraction may be necessary to resolve the overlap.

A fit of the normalized count data and the chemistry data for aluminum was obtained for 63 data points. Based on the Cook's Distance diagnostic, two data points were identified as potential outliers that were significantly different from the bulk of the data. Both data points, which have a high value of *C* with respect to *PG*, were removed from the data set.

A plot of the calibration equation with uncertainties for the gamma-ray peak at 1.524 MeV is provided in Figure A.12 of Appendix A. The regression line is given by

$$C_K = 1.362 \times 10^7 \cdot PG_{1.524\,MeV} \tag{25}$$

Additional gamma-ray-peaks for potassium are reported in the literature, but their relative intensity and, therefore, their sensitivity are an order of magnitude lower. None of these gamma-ray peaks were observed in the gamma-spectra for the standards due to the low sensitivity of potassium.

Elements without a Calibration

A number of light elements are reported in the literature to produce gamma-ray peaks from alpha-particle induced reactions, but insufficient data was available to obtain a fit. Elements such as lithium, boron, and silicon were not present in a sufficient number of standards to obtain a fit. Other elements such as nitrogen were not incorporated as part of the solid material matrix and, therefore, not detected in the materials. Although oxygen was incorporated as part of the material matrix, the only isotopes detectable were ^{17}O and ^{18}O, which are present in very low abundance making detection unreliable. A description of the available data for each of these elements is presented below.

Lithium

Naturally occurring isotopes of lithium include ^{6}Li and ^{7}Li. Alpha-particle-induced reactions with lithium produce a single gamma-ray peak at 0.478 MeV from the alpha-scattering reaction

^{7}Li(α,α'γ). Although this gamma-ray peak is in the low-energy region of the spectrum, which is heavily populated with actinide gamma-rays, the ROI for this gamma-ray peak is relatively free of interference. Lithium was detected in only three of the standards, and a fit of the data could not be obtained.

Boron

Naturally occurring isotopes of lithium include ^{10}B and ^{11}B. Multiple gamma-ray peaks produced from alpha-particle-induced reactions with both ^{10}B and ^{11}B are reported in the literature. However, in the standards a single gamma-ray peak at 3.684 MeV from the ^{10}B(α,pγ) reaction was observed. Boron was detected in only three of the standards, and a fit of the data could not be obtained.

Oxygen

Naturally occurring isotopes of oxygen include ^{16}O, ^{17}O, and ^{18}O, however only ^{17}O and ^{18}O are involved in alpha-particle-induced reactions. Due to the low abundance of ^{17}O and ^{18}O (0.04% and 0.2% respectively), the overall sensitivity of the method to detection of oxygen is much lower than many of the other elements. In pure PuO_2, gamma-ray peaks from alpha-particle induced reactions were observed at 1.634 MeV from the ^{17}O(α,nγ) reaction and at 2.438 MeV from the ^{17}O(α,nγ) reaction.

Gamma-ray spectra from two classes of packaged materials, pure plutonium oxide from metal oxidation and plutonium oxide produced from the magnesium hydroxide precipitation process, were analyzed to determine whether the gamma-ray peaks for oxygen may be used quantitatively. The pure plutonium oxide class averaged about 86.8% plutonium and 12.8 % oxygen, and the class of oxide produced by magnesium hydroxide precipitation had on the average 54.2% plutonium and 22.5% oxygen. The higher concentration in the latter class was due to the presence of other non-actinide oxides, mainly MgO. The results showed that the signal from 1.634 MeV gamma-ray peak was the about the same for both classes of materials, which indicates that the alpha-particle-induced reactions are occurring with only the oxygen present in the actinide (plutonium and americium) oxide. Therefore, a fit could not be obtained from the standards because the concentration of oxygen undergoing alpha-particle-induced reactions in the material is controlled by the amount of oxygen present in plutonium oxide, which is about the same for all materials.

Silicon

Naturally occurring isotopes of silicon include ^{28}Si, ^{29}Si, and ^{30}Si. Multiple gamma-ray peaks produced from alpha-particle-induced reactions with all three isotopes are reported in the literature. However, the most intense gamma-ray peak at 0.078 MeV cannot be used because it is located in the heavily filtered, low-energy region of the spectrum. The remaining peaks occur in the region of the spectrum above 1 MeV, but they all overlap those of other elements including aluminum and magnesium. The most intense of these gamma-ray peaks occurs at 2.234 MeV from the ^{28}Si(α,pγ)^{31}P reaction, which overlaps the highest intensity gamma-ray peak for aluminum. The data for the standards indicated that the signal in this region was a

response to aluminum and not silicon. Because the standards did not include any materials high in silicon and low in aluminum, a fit for silicon could not be obtained.

Nitrogen

Naturally occurring isotopes of nitrogen include ^{14}N and ^{15}N. A single gamma-ray peak from alpha-particle-induced reactions with ^{14}N are reported in the literature at 0.871 MeV from the $^{14}N(\alpha,p\gamma)^{17}O$ reaction. The reactions only occur with nitrogen in solid compounds within the material matrix. Gamma-ray peaks originating from gas-phase reactions with nitrogen have not been observed or reported. Although solid nitrogen compounds, such as nitrates, are present in some materials, the concentrations of these compounds are likely below detectable levels.

Conclusion

This report documents the new PG calibration regression equation. These calibration equations incorporate new data that have become available since revision 1 of "A Calibration to Predict the Concentrations of Impurities in Plutonium Oxide by Prompt Gamma Analysis" was issued [3] The calibration equations are based on a weighted least squares (WLS) approach for the regression. The WLS method gives each data point its proper amount of influence over the parameter estimates. This gives two big advantages, more precise parameter estimates and better and more defensible estimates of uncertainties. The WLS approach makes sense both statistically and experimentally because the variances increase with concentration, and there are physical reasons that the higher measurements are less reliable and should be less influential.

The new magnesium calibration includes a correction for sodium and separate calibration equation for items with and without chlorine. These additional calibration equations allow for better predictions and smaller uncertainties for sodium in materials with and without chlorine. Chlorine and sodium have separate equations for RICH materials. Again, these equations give better predictions and smaller uncertainties chlorine and sodium for RICH materials.

References

1. McKibben, M. 1968. Reaction Gammas for Analysis of Impurities in Alpha Emitters, *Nuclear Applications* 4, 260-267.

2. Martin, R. H. 1975. *Reaction Gamma-Rays in Plutonium Compounds, Mixtures, and Alloys,* Dow Chemical, USA, Rocky Flats Division, (RFP-2382).

3. Narlesky, J. E., Foster, L. A., Kelly, E. J., and Murray, Roy, E. 2009. *A Calibration to Predict the Concentrations of Impurities in Plutonium Oxide by Prompt Gamma Analysis: Revision 1*. Los Alamos National Laboratory, (LA-14411).

4. Lavagnini, L. and F. Magno. 2006. A Statistical Overview on Univariate Calibration, Inverse Regression, and Detection Limits: Application to Gas Chromatography/Mass Spectrometry Technique. Published online 20 June 2006 in Wiley InterScience (www.interscience.wiley.com) DOI 10.1002/mas.20100.

5. Massart, L.M, Vandenginste, B.G.M., Buydens, L.M.C., De Jong, S., Lewi, P.J., Smeyers-Verbeke, J. 1997. Handbook of Chemometrics and Qualimetrics: Part A, Elsevier, Amsterdam.

6. Giles, I. S. and M. Peisach. 1979. A Survey of the Analytical Significance of Prompt-Gamma Rays Induced by 5 MeV Alpha-Particles, *Journal of Radioanalytic Nuclear Chemistry,* 50, 307-360.

7. Narlesky, J. E. 2009. *Prompt Gamma Analysis Software Version 4.7 User's Guide.* Los Alamos National Laboratory, (LA-UR-09-04712).

Appendix A. Calibration Plots

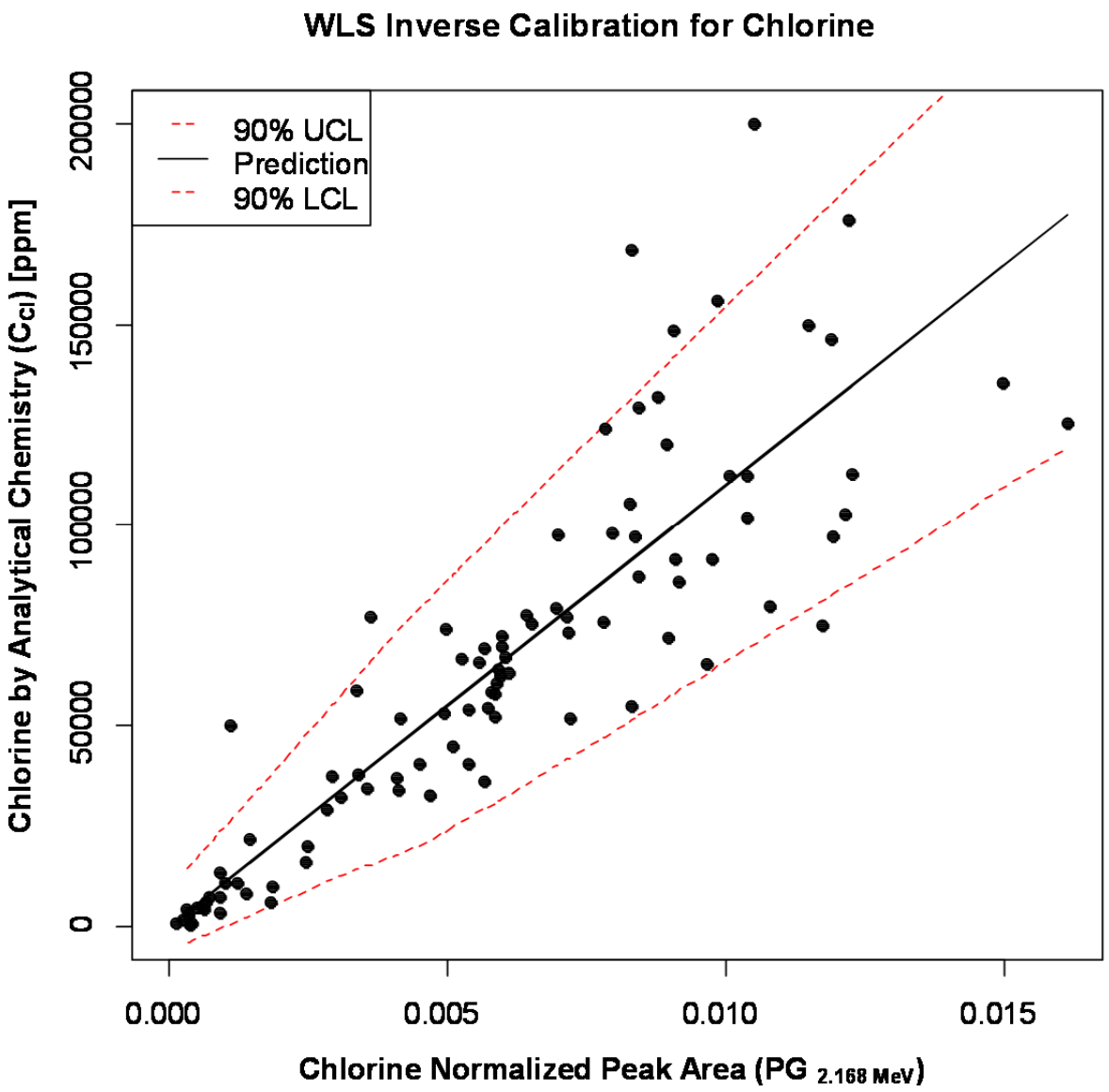

FIGURE A.1. CALIBRATION EQUATION FOR CHLORINE USING ALL DATA. SOLID LINE IS CALIBRATION LINE AND DASHED LINES ARE UNCERTAINTIES.

TABLE A.1. CHLORINE CALIBRATION PARAMETERS AND UPPER AND LOWER CONFIDENCE INTERVALS (UCL / LCL) CALCULATED FOR THE DATA SET MINIMUM, MIDPOINT, AND MAXIMUM.

	n	*df*	β	PG_0	C_0	*LCL(90%)*	*UCL(90%)*	*LCL(95%)*	*UCL(95%)*
			[ppm^{-1}]		[ppm]	[ppm]	[ppm]	[ppm]	[ppm]
Data Set Minimum	94	93	9.096E-08	1.19E-04	**1.3E+03**	0.0E+00	6.4E+03	0.0E+00	7.4E+03
Data Set Midpoint	94	93	9.096E-08	8.12E-03	**8.9E+04**	5.0E+04	1.3E+05	5.0E+04	1.4E+05
Data Set Maximum	94	93	9.096E-08	1.61E-02	**1.8E+05**	1.2E+05	2.3E+05	1.2E+05	2.4E+05

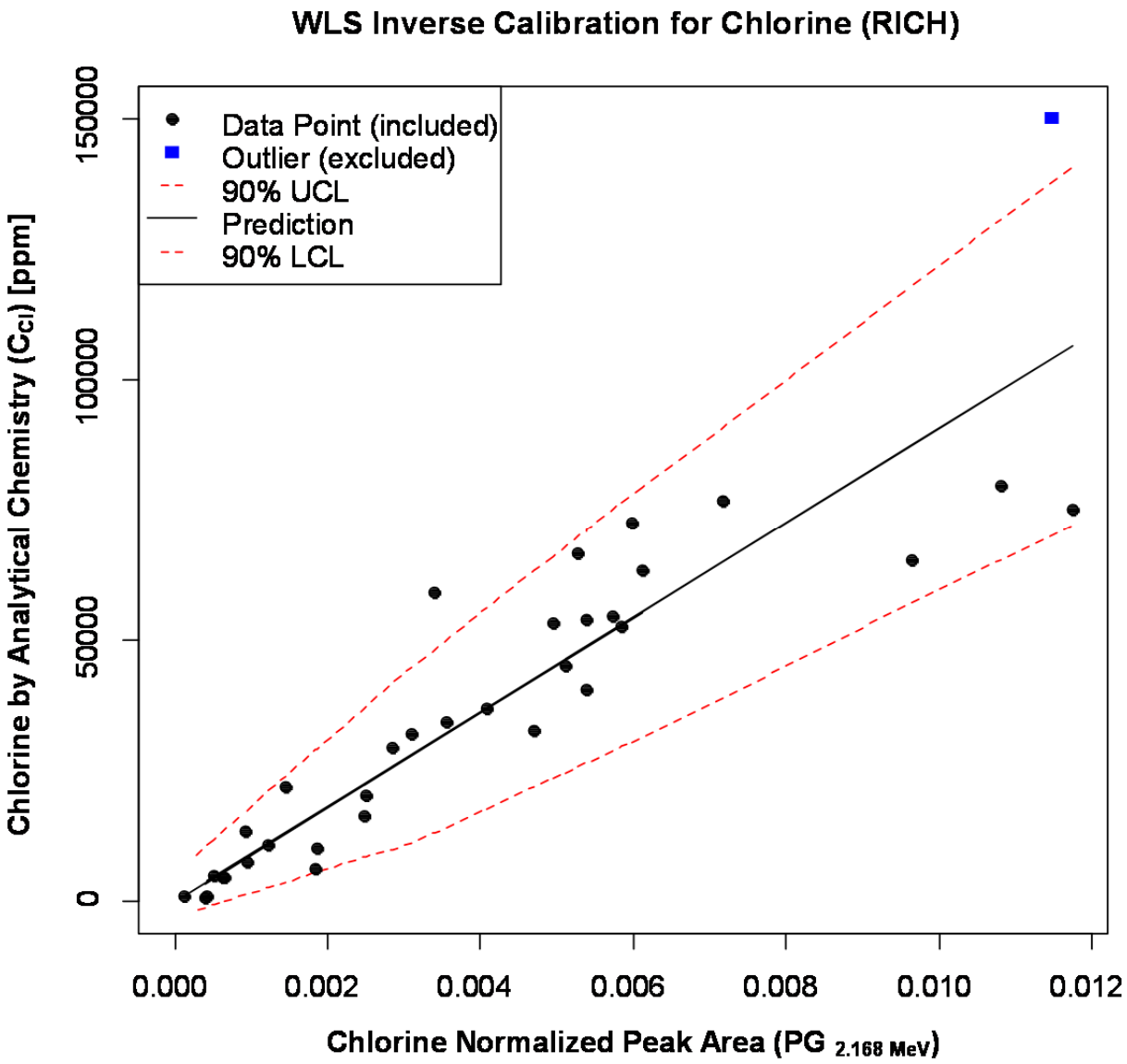

FIGURE A.2. CALIBRATION EQUATION FOR CHLORINE USING RICH DATA EXCEPT FOR ONE OUTLIER (BLUE SQUARES). SOLID LINE IS CALIBRATION LINE AND DASHED LINES ARE UNCERTAINTIES.

TABLE A.2. CHLORINE RICH CALIBRATION PARAMETERS AND UPPER AND LOWER CONFIDENCE INTERVALS (UCL / LCL) CALCULATED FOR THE DATA SET MINIMUM, MIDPOINT, AND MAXIMUM.

	n	*df*	*β*	*PG 0*	*C 0*	*LCL(90%)*	*UCL(90%)*	*LCL(95%)*	*UCL(95%)*
			[ppm^{-1}]		[ppm]	[ppm]	[ppm]	[ppm]	[ppm]
Data Set Minimum	33	32	1.103E-07	1.19E-04	**1.1E+03**	0.0E+00	4.7E+03	0.0E+00	5.4E+03
Data Set Midpoint	33	32	1.103E-07	5.93E-03	**5.4E+04**	3.0E+04	7.7E+04	3.0E+04	8.2E+04
Data Set Maximum	33	32	1.103E-07	1.17E-02	**1.1E+05**	7.2E+04	1.4E+05	7.2E+04	1.5E+05

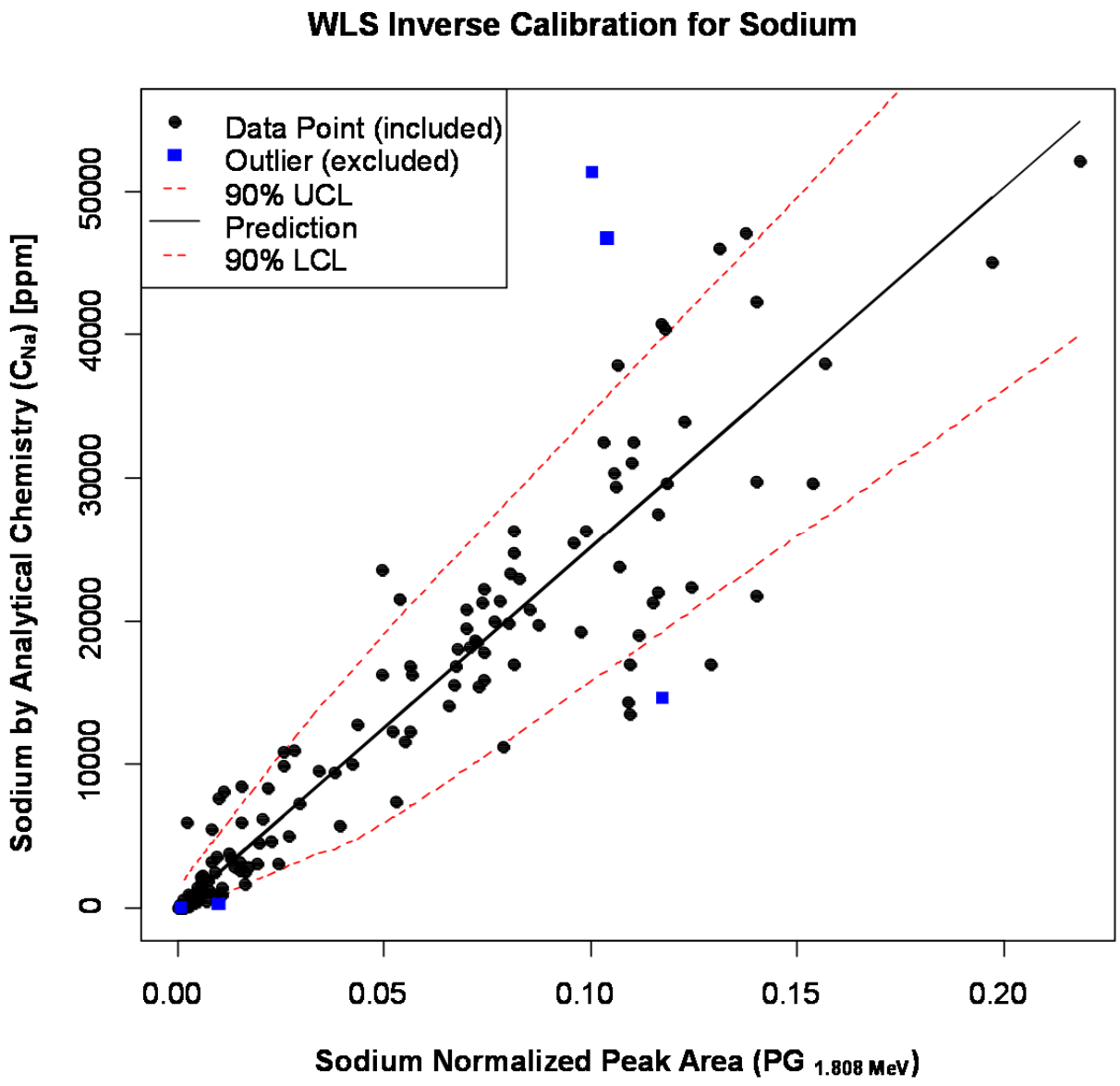

FIGURE A.3. CALIBRATION EQUATION FOR SODIUM USING ALL DATA EXCEPT FOR OUTLIERS (BLUE SQUARES). SOLID LINE IS CALIBRATION LINE AND DASHED LINES ARE UNCERTAINTIES.

TABLE A.3. SODIUM CALIBRATION PARAMETERS AND UPPER AND LOWER CONFIDENCE INTERVALS (UCL / LCL) CALCULATED FOR THE DATA SET MINIMUM, MIDPOINT, AND MAXIMUM.

	n	*df*	*β*	*PG 0*	*C 0*	*LCL(90%)*	*UCL(90%)*	*LCL(95%)*	*UCL(95%)*
			[ppm^{-1}]		[ppm]	[ppm]	[ppm]	[ppm]	[ppm]
Data Set Minimum	145	144	3.977E-06	3.19E-04	**8.0E+01**	0.0E+00	6.3E+02	0.0E+00	7.3E+02
Data Set Midpoint	145	144	3.977E-06	1.09E-01	**2.7E+04**	1.8E+04	3.7E+04	1.8E+04	3.9E+04
Data Set Maximum	145	144	3.977E-06	2.18E-01	**5.5E+04**	4.1E+04	6.9E+04	4.1E+04	7.2E+04

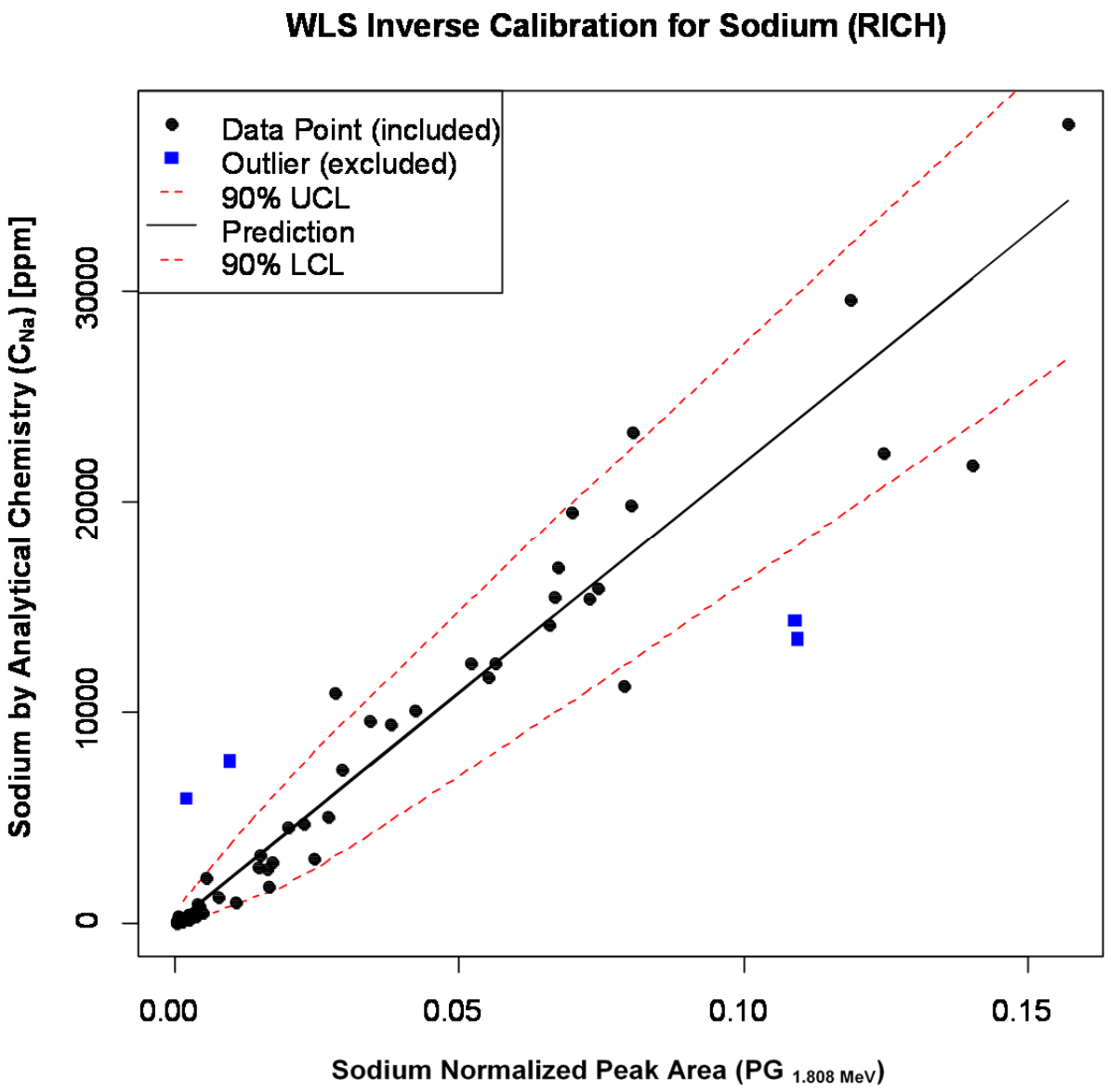

FIGURE A.4. CALIBRATION EQUATION FOR SODIUM USING RICH DATA EXCEPT FOR OUTLIERS (BLUE SQUARES). SOLID LINE IS CALIBRATION LINE AND DASHED LINES ARE UNCERTAINTIES.

TABLE A.4. SODIUM RICH CALIBRATION PARAMETERS AND UPPER AND LOWER CONFIDENCE INTERVALS (UCL / LCL) CALCULATED FOR THE DATA SET MINIMUM, MIDPOINT, AND MAXIMUM.

	n	*df*	*β*	*PG 0*	*C 0*	*LCL(90%)*	*UCL(90%)*	*LCL(95%)*	*UCL(95%)*
			[ppm^{-1}]		[ppm]	[ppm]	[ppm]	[ppm]	[ppm]
Data Set Minimum	54	53	4.568E-06	3.19E-04	**7.0E+01**	0.0E+00	4.0E+02	0.0E+00	4.7E+02
Data Set Midpoint	54	53	4.568E-06	7.86E-02	**1.7E+04**	1.2E+04	2.2E+04	1.2E+04	2.3E+04
Data Set Maximum	54	53	4.568E-06	1.57E-01	**3.4E+04**	2.7E+04	4.2E+04	2.7E+04	4.3E+04

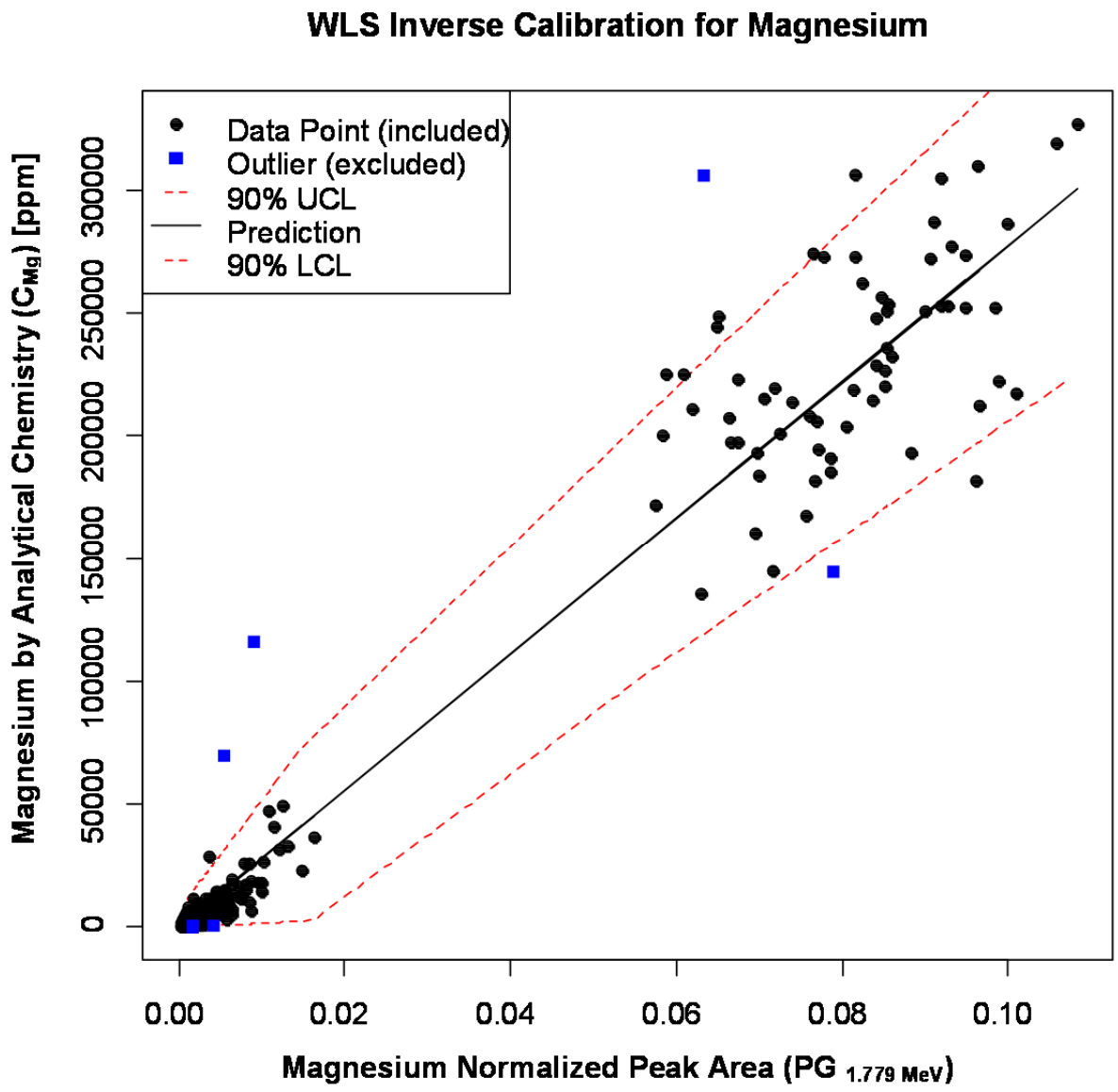

FIGURE A.5. CALIBRATION EQUATION FOR MAGNESIUM USING ALL DATA EXCEPT FOR OUTLIERS (BLUE SQUARES). SOLID LINE IS CALIBRATION LINE AND DASHED LINES ARE UNCERTAINTIES.

TABLE A.5. MAGNESIUM CALIBRATION PARAMETERS AND UPPER AND LOWER CONFIDENCE INTERVALS (UCL / LCL) CALCULATED FOR THE DATA SET MINIMUM, MIDPOINT, AND MAXIMUM.

	n	*df*	*β*	*PG 0*	*C 0*	*LCL(90%)*	*UCL(90%)*	*LCL(95%)*	*UCL(95%)*
			[ppm^{-1}]		[ppm]	[ppm]	[ppm]	[ppm]	[ppm]
Data Set Minimum	182	181	3.606E-07	3.00E-04	**8.3E+02**	0.0E+00	4.7E+03	0.0E+00	5.5E+03
Data Set Midpoint	182	181	3.606E-07	5.43E-02	**1.5E+05**	9.8E+04	2.0E+05	9.8E+04	2.1E+05
Data Set Maximum	182	181	3.606E-07	1.08E-01	**3.0E+05**	2.3E+05	3.7E+05	2.3E+05	3.9E+05

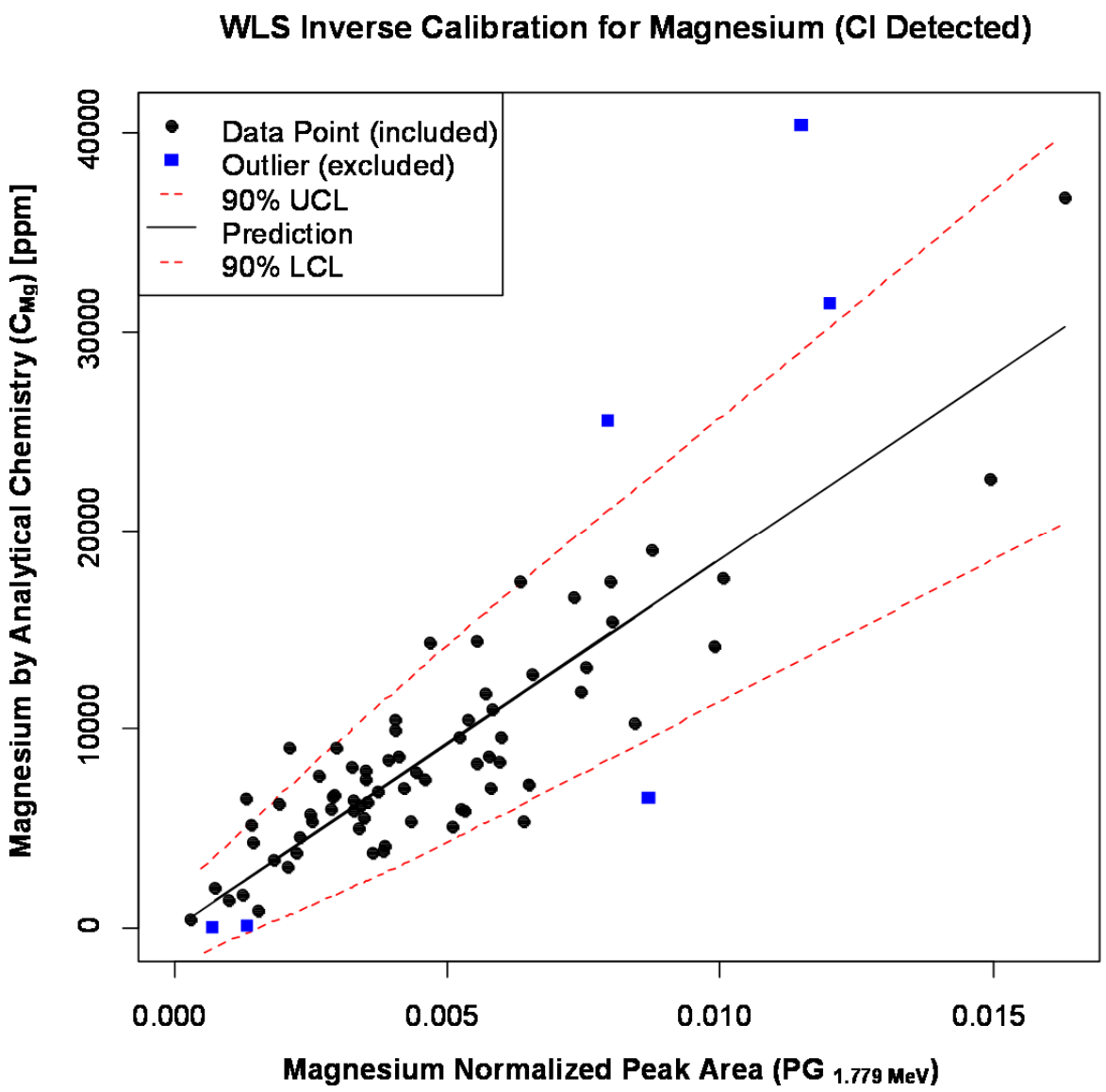

FIGURE A.6. CALIBRATION EQUATION FOR MAGNESIUM RESTRICTED TO MATERIALS WITH CHLORINE DETECTED AND EXCLUDING OUTLIERS (BLUE SQUARES). SOLID LINE IS CALIBRATION LINE AND DASHED LINES ARE UNCERTAINTIES.

TABLE A.6. MAGNESIUM (WITH CHLORINE) CALIBRATION PARAMETERS AND UPPER AND LOWER CONFIDENCE INTERVALS (UCL / LCL) CALCULATED FOR THE DATA SET MINIMUM, MIDPOINT, AND MAXIMUM.

	n	*df*	β	PG_0	C_0	*LCL(90%)*	*UCL(90%)*	*LCL(95%)*	*UCL(95%)*
			[ppm^{-1}]		[ppm]	[ppm]	[ppm]	[ppm]	[ppm]
Data Set Minimum	71	70	5.394E-07	3.00E-04	**5.6E+02**	0.0E+00	1.9E+03	0.0E+00	2.2E+03
Data Set Midpoint	71	70	5.394E-07	8.30E-03	**1.5E+04**	9.0E+03	2.2E+04	9.0E+03	2.3E+04
Data Set Maximum	71	70	5.394E-07	1.63E-02	**3.0E+04**	2.1E+04	3.9E+04	2.1E+04	4.1E+04

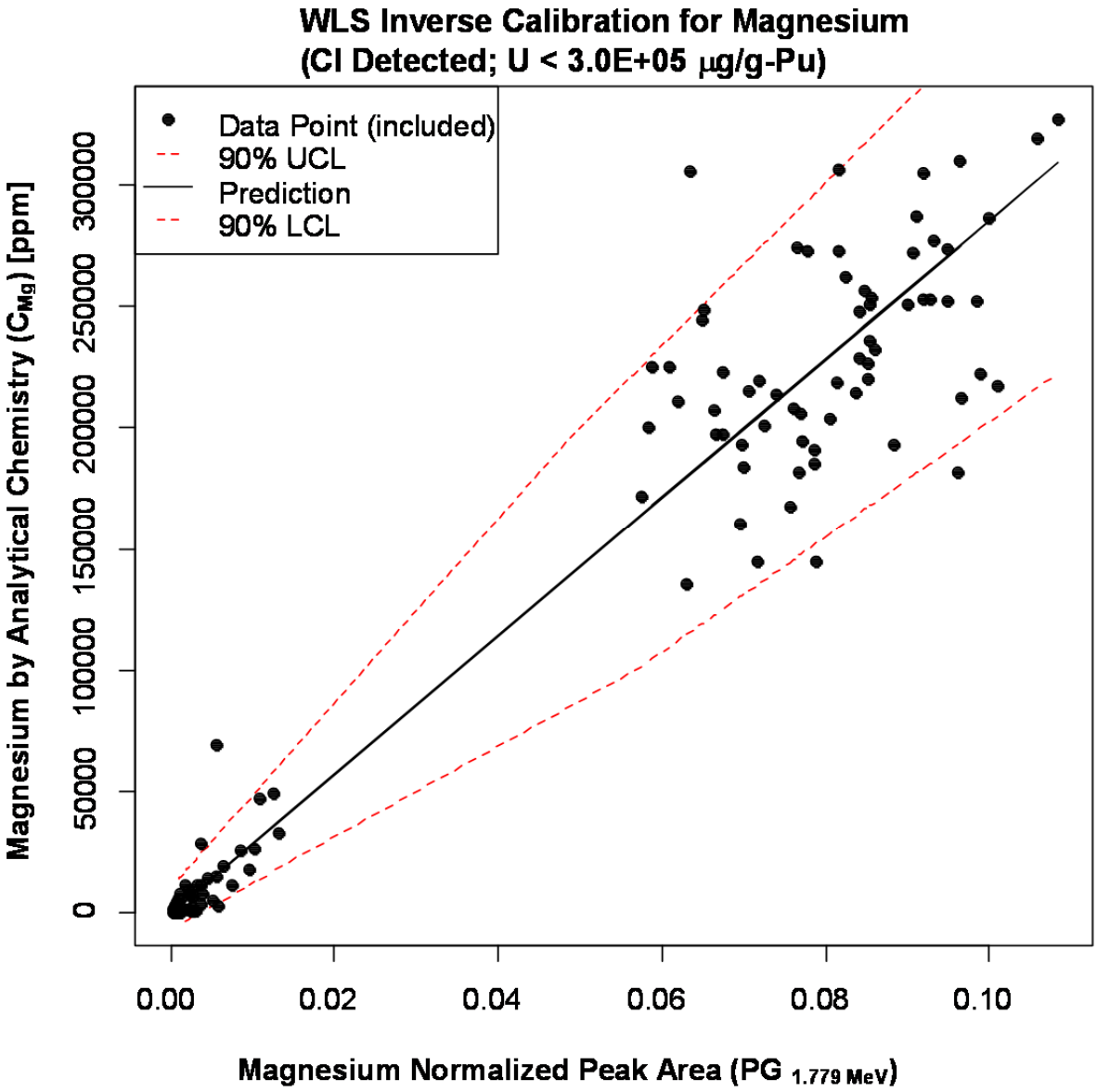

FIGURE A.7. CALIBRATION EQUATION FOR MAGNESIUM RESTRICTED TO MATERIALS WITHOUT CHLORINE DETECTED. SOLID LINE IS CALIBRATION LINE AND DASHED LINES ARE UNCERTAINTIES. THE DATA WITHOUT CHLORINE DETECTED ARE ALSO RESTRICTED TO URANIUM<30%.

TABLE A.7. MAGNESIUM (WITHOUT CHLORINE AND RESTRICTED TO URANIUM<30%.) CALIBRATION PARAMETERS AND UPPER AND LOWER CONFIDENCE INTERVALS (UCL / LCL) CALCULATED FOR THE DATA SET MINIMUM, MIDPOINT, AND MAXIMUM.

	n	*df*	*β*	PG_0	C_0	*LCL(90%)*	*UCL(90%)*	*LCL(95%)*	*UCL(95%)*
			[ppm^{-1}]		[ppm]	[ppm]	[ppm]	[ppm]	[ppm]
Data Set Minimum	104	103	3.544E-07	3.13E-04	**8.8E+02**	0.0E+00	5.0E+03	0.0E+00	5.8E+03
Data Set Midpoint	104	103	3.544E-07	5.43E-02	**1.5E+05**	1.0E+05	2.1E+05	1.0E+05	2.2E+05
Data Set Maximum	104	103	3.544E-07	1.08E-01	**3.1E+05**	2.3E+05	3.8E+05	2.3E+05	4.0E+05

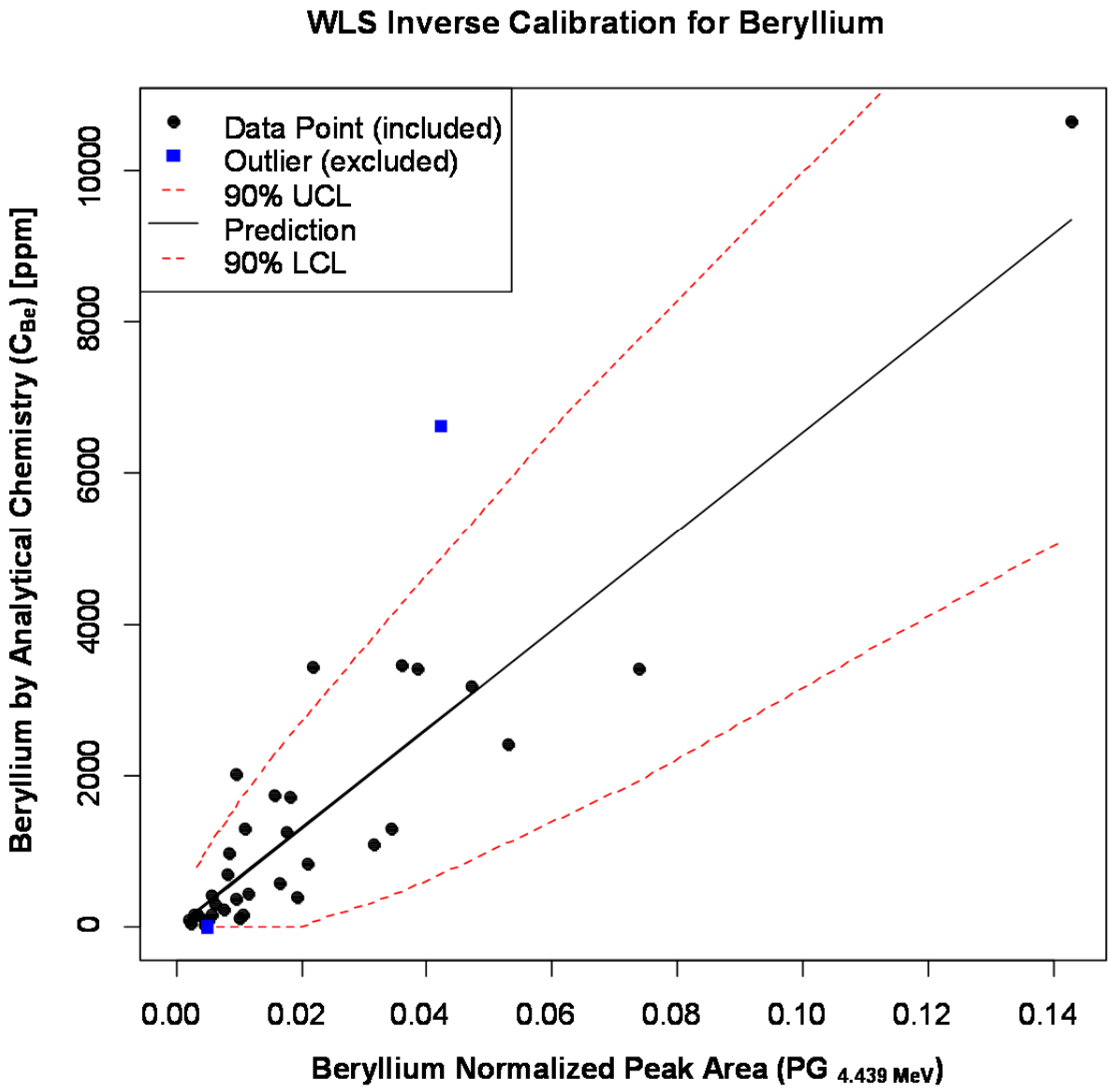

FIGURE A.8. CALIBRATION EQUATION FOR BERYLLIUM BASED ON ALL DATA AND EXCLUDING OUTLIERS (BLUE SQUARES). SOLID LINE IS CALIBRATION LINE AND DASHED LINES ARE UNCERTAINTIES.

TABLE A.8. BERYLLIUM CALIBRATION PARAMETERS AND UPPER AND LOWER CONFIDENCE INTERVALS (UCL / LCL) CALCULATED FOR THE DATA SET MINIMUM, MIDPOINT, AND MAXIMUM.

	n	*df*	β	PG_0	C_0	*LCL(90%)*	*UCL(90%)*	*LCL(95%)*	*UCL(95%)*
			[ppm^{-1}]		[ppm]	[ppm]	[ppm]	[ppm]	[ppm]
Data Set Minimum	34	33	1.527E-05	2.05E-03	**1.3E+02**	0.0E+00	6.0E+02	0.0E+00	6.9E+02
Data Set Midpoint	34	33	1.527E-05	7.24E-02	**4.7E+03**	1.9E+03	7.5E+03	1.9E+03	8.1E+03
Data Set Maximum	34	33	1.527E-05	1.43E-01	**9.3E+03**	5.2E+03	1.3E+04	5.2E+03	1.4E+04

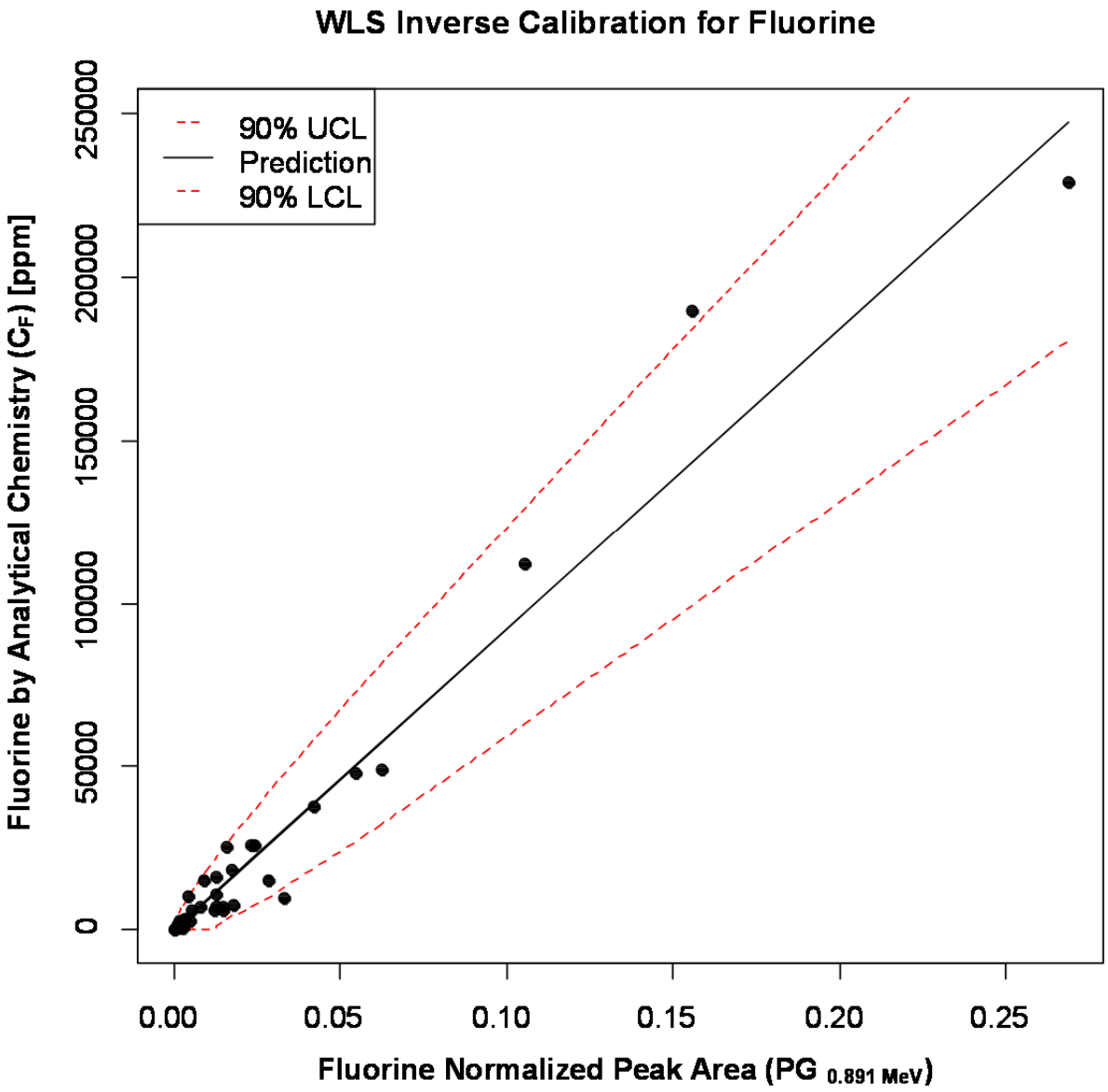

FIGURE A.9. CALIBRATION EQUATION FOR FLUORINE BASED ON ALL DATA. SOLID LINE IS CALIBRATION LINE AND DASHED LINES ARE UNCERTAINTIES.

TABLE A.9. FLUORINE CALIBRATION PARAMETERS AND UPPER AND LOWER CONFIDENCE INTERVALS (UCL / LCL) CALCULATED FOR THE DATA SET MINIMUM, MIDPOINT, AND MAXIMUM.

	n	*df*	*β*	PG_0	C_0	*LCL(90%)*	*UCL(90%)*	*LCL(95%)*	*UCL(95%)*
			[ppm^{-1}]		[ppm]	[ppm]	[ppm]	[ppm]	[ppm]
Data Set Minimum	38	37	1.084E-06	1.16E-04	**1.1E+02**	0.0E+00	1.4E+03	0.0E+00	1.6E+03
Data Set Midpoint	38	37	1.084E-06	1.34E-01	**1.2E+05**	8.6E+04	1.6E+05	8.6E+04	1.7E+05
Data Set Maximum	38	37	1.084E-06	2.69E-01	**2.5E+05**	1.9E+05	3.0E+05	1.9E+05	3.2E+05

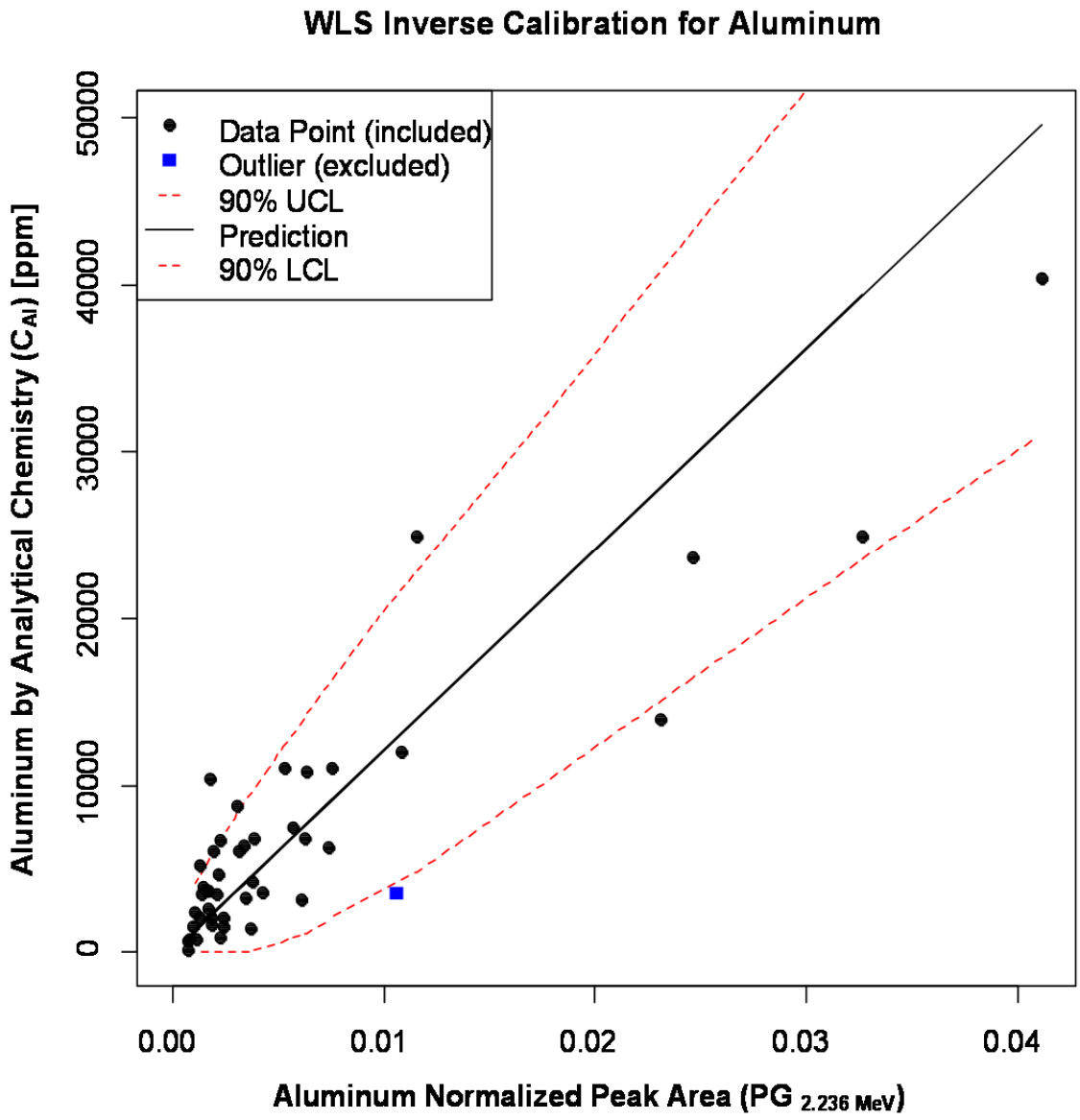

FIGURE A.10. CALIBRATION EQUATION FOR ALUMINUM BASED ON ALL DATA EXCLUDING ONE OUTLIER (BLUE SQUARE). SOLID LINE IS CALIBRATION LINE AND DASHED LINES ARE UNCERTAINTIES.

TABLE A.10. ALUMINUM CALIBRATION PARAMETERS AND UPPER AND LOWER CONFIDENCE INTERVALS (UCL / LCL) CALCULATED FOR THE DATA SET MINIMUM, MIDPOINT, AND MAXIMUM.

	n	*df*	*β*	*PG 0*	*C 0*	*LCL(90%)*	*UCL(90%)*	*LCL(95%)*	*UCL(95%)*
			[ppm^{-1}]		[ppm]	[ppm]	[ppm]	[ppm]	[ppm]
Data Set Minimum	44	43	8.282E-07	7.52E-04	**9.1E+02**	0.0E+00	3.2E+03	0.0E+00	3.7E+03
Data Set Midpoint	44	43	8.282E-07	2.09E-02	**2.5E+04**	1.3E+04	3.8E+04	1.3E+04	4.0E+04
Data Set Maximum	44	43	8.282E-07	4.11E-02	**5.0E+04**	3.1E+04	6.8E+04	3.1E+04	7.1E+04

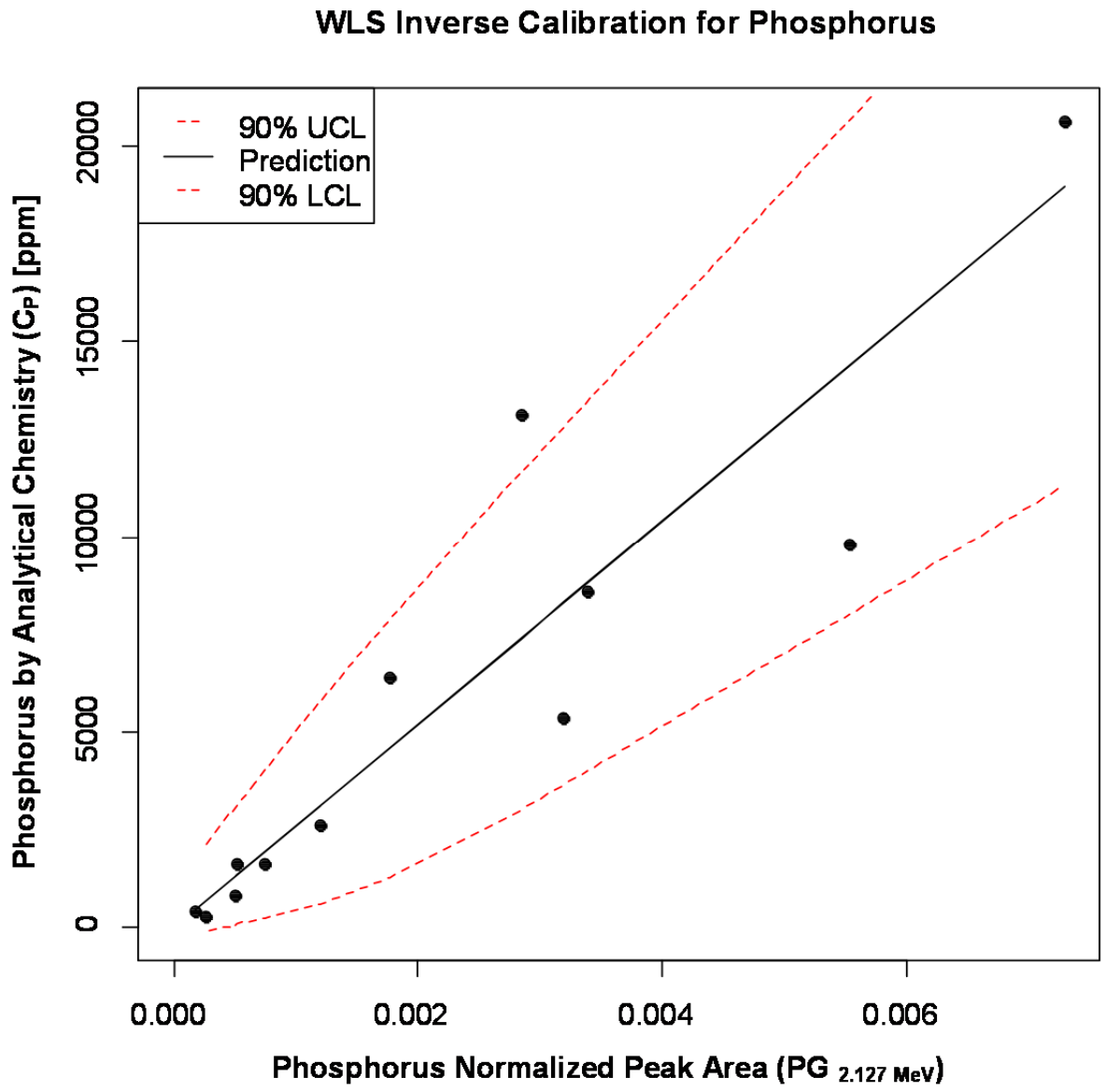

FIGURE A.11. CALIBRATION EQUATION FOR PHOSPHOROUS BASED ON ALL DATA. SOLID LINE IS CALIBRATION LINE AND DASHED LINES ARE UNCERTAINTIES.

TABLE A.11. PHOSPHORUS CALIBRATION PARAMETERS AND UPPER AND LOWER CONFIDENCE INTERVALS (UCL / LCL) CALCULATED FOR THE DATA SET MINIMUM, MIDPOINT, AND MAXIMUM.

	n	*df*	β	PG_0	C_0	*LCL(90%)*	*UCL(90%)*	*LCL(95%)*	*UCL(95%)*
			[ppm^{-1}]		[ppm]	[ppm]	[ppm]	[ppm]	[ppm]
Data Set Minimum	12	11	3.842E-07	1.75E-04	**4.6E+02**	0.0E+00	1.6E+03	0.0E+00	1.9E+03
Data Set Midpoint	12	11	3.842E-07	3.73E-03	**9.7E+03**	4.7E+03	1.5E+04	4.7E+03	1.6E+04
Data Set Maximum	12	11	3.842E-07	7.29E-03	**1.9E+04**	1.1E+04	2.7E+04	1.1E+04	2.8E+04

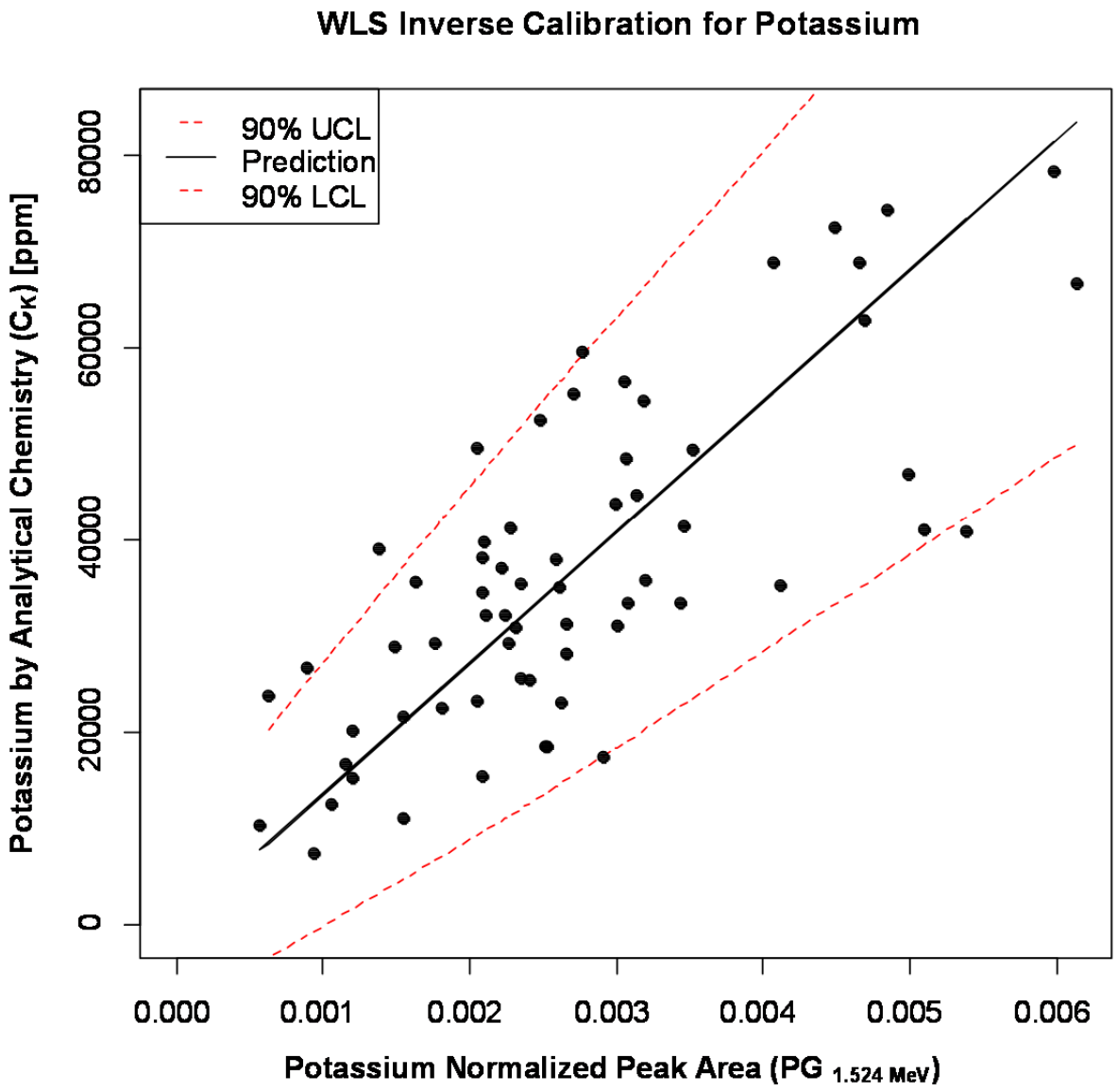

FIGURE A.12. CALIBRATION EQUATION FOR POTASSIUM BASED ON ALL DATA. SOLID LINE IS CALIBRATION LINE AND DASHED LINES ARE UNCERTAINTIES.

TABLE A.12. POTASSIUM CALIBRATION PARAMETERS AND UPPER AND LOWER CONFIDENCE INTERVALS (UCL / LCL) CALCULATED FOR THE DATA SET MINIMUM, MIDPOINT, AND MAXIMUM.

	n	*df*	β	PG_0	C_0	*LCL(90%)*	*UCL(90%)*	*LCL(95%)*	*UCL(95%)*
			[ppm^{-1}]		[ppm]	[ppm]	[ppm]	[ppm]	[ppm]
Data Set Minimum	63	62	7.340E-08	5.71E-04	**7.8E+03**	0.0E+00	1.8E+04	0.0E+00	2.0E+04
Data Set Midpoint	63	62	7.340E-08	3.35E-03	**4.6E+04**	2.2E+04	7.0E+04	2.2E+04	7.4E+04
Data Set Maximum	63	62	7.340E-08	6.13E-03	**8.4E+04**	5.0E+04	1.2E+05	5.0E+04	1.2E+05

Appendix B. Parameters for Calibration Equations and Uncertainty Calculation

Calibration	Eq. No.	Applicability	*n*	*df*	β [ppm^{-1}]	*se*	Σw_i	$\Sigma w_i C_i^2$ [ppm^2]	$(\Sigma w_i C_i)^2$ [ppm^2]	$\overline{PG_w}$	*t (df,0.05)*
C_{Al}	23	*Full Data Set*	44	43	8.282E-07	3.654E-05	2.132E-02	3.071E+05	44	2.008E-03	1.6802
C_{Be}	21	*Full Data Set*	34	33	1.527E-05	3.503E-04	1.388E-01	4.685E+04	34	6.861E-03	1.6909
C_{Cl}	13	*Full Data Set*	94	93	9.096E-08	7.223E-06	7.863E-03	6.074E+06	94	1.340E-03	1.6612
C_{Cl} *(RICH)*	14	*RICH Data Set*	33	32	1.103E-07	6.477E-06	5.228E-03	1.148E+06	33	8.932E-04	1.6924
C_{F}	22	*Full Data Set*	38	37	1.084E-06	6.503E-05	2.187E-02	9.088E+05	38	2.510E-03	1.6860
C_{Mg} *(corr.)*	18	*Full Data Set; Na Correction*	182	181	3.606E-07	2.921E-05	6.719E-02	1.560E+07	182	1.844E-03	1.6533
C_{Mg} *(Cl; corr.)*	19	*Cl detected; Na Correction*	71	70	5.394E-07	1.654E-05	1.432E-02	6.110E+05	71	2.901E-03	1.6666
C_{Mg} *(No Cl; corr.)*	20	*Cl NOT detected; Na Correction*	104	103	3.544E-07	2.878E-05	2.802E-02	1.503E+07	104	1.989E-03	1.6596
C_{P}	24	*Full Data Set*	12	11	3.842E-07	1.040E-05	9.523E-03	7.128E+04	12	5.894E-04	1.7823
C_{K}	25	*Full Data Set*	63	62	7.340E-08	4.862E-06	2.208E-03	2.320E+06	63	2.236E-03	1.6694
C_{Na}	15	*Full Data Set*	145	144	3.977E-06	1.429E-04	2.787E-01	1.802E+06	145	2.805E-03	1.6554
C_{Na} *(RICH)*	16	*RICH Data Set*	54	53	4.568E-06	1.035E-04	1.557E-01	3.886E+05	54	2.242E-03	1.6736